Analysis of localization phenomena in Shape Memory Alloys bars by a variational approach

Roberto Alessi[a], Davide Bernardini[b,*]

[a] *Department of Structural and Geotechnical Engineering, University of Rome Sapienza, Via Eudossiana 18, 00184, Roma, Italy*
[b] *Department of Structural and Geotechnical Engineering, University of Rome Sapienza, Via Antonio Gramsci 53, 00197, Roma, Italy*

Abstract

Localization of the phase transformations in Shape Memory Alloys (SMA) wires are well known. Several experimental and theoretical studies appeared in the last years. In this work the problem is addressed by means of a variational approach within the framework of the modeling of rate-independent materials by the specification of a non-local free energy and a dissipation function, focusing attention on the basic case of isothermal conditions. General expressions are given for a rather broad class of models, whereas a simple model is studied in detail. A full stability analysis of both homogeneous and non-homogeneous solutions is carried out analytically, showing that stable non-homogeneous solutions have necessarily to occur if the bar is longer than an internal length determined by the constitutive parameters. The analysis also shows that snap-back phenomena may occur both in the nucleation and the coalescence phase, depending on another material length which is also function of the number of transformation fronts. This helps to explain why the second stress drop associated to coalescence is much more difficult to observe experimentally. Closed form expressions are given for the phase fraction profiles of both single and multiple localizations as well as nucleation and propagation stresses. A comparison between the prediction of the model with experimental data finally shows a good agreement both in terms of global response and in the spatio-temporal evolution of the transformation domains.

Keywords: shape memory alloys, phase transformations, energetic formulation, variational approach, nonlocal model, material stability

Dedicated to the memory of Robert F. C. Walters.

*Corresponding author
Email addresses: roberto.alessi@uniroma1.it (Roberto Alessi), davide.bernardini@uniroma1.it (Davide Bernardini)

1. Introduction

Shape Memory Alloys (SMA) exhibit a complex thermomechanical behavior induced by the occurrence of phase transformations between austenite and one or more variants or groups of variants of martensite [33, 23]. This is reflected at the macroscopic scale by their peculiar functional properties known as pseudoelasticity, one or two-way shape memory effect [22, 26]. Such properties are nowadays widely known and are exploited by an increasing number of applications like, among the others: biomedical devices, aerospace structures, mechanical components, MEMS as well as civil engineering structural elements or devices [40, 41].

While the basic properties of SMA were known since 1960s, Shaw and Kyriakides [45] first noticed the occurrence of non-homogeneous strain fields associated with the localization of the phase transformations at the macroscopic scale in NiTi superelastic wires. Further experimental investigations then provided ample confirmation that, during tensile tests under displacement control, NiTi wires or stripes tend to transform through the nucleation, growth and propagation of macroscopic domains observable at the macroscopic scale in the form of bands with striking similarity with Lüders phenomena observed in other types of metals [46, 43, 21, 11]. This phenomenology was confirmed by Sun and coworkers in fine-grained polycrystalline NiTi microtubes where an additional level of complexity arises with respect to the possibility of formation of cylindrical or helix-shaped domains [49, 16, 18]. Recent experiments show qualitatively similar behavior also for SMA tubes subject to bending [4].

Further experimental analyses pointed out the importance of the thermomechanical coupling [21, 42, 50, 13]. The latent heat released or absorbed during phase transformations is localized at the domains and this generates a non-uniform temperature field that, given the temperature dependence of the nucleation stress, usually gives rise to the formation of multiple domains. Since the actual temperature field is determined by the concomitant effect of the latent heat and the heat exchanged with the environment, the thermomechanical coupling is strongly related to the loading rate. For each loading rate the maximum number of fronts and the corresponding spacing has been estimated in [20].

The occurrence of localized phase transformations is reflected on the overall response of the sample by stress peaks that can be interpreted as the difference between the nucleation and propagation stresses emerging as an outcome of material instability. The fact that SMA tend to show unstable softening behavior is known since the first thermodynamic equilibrium analyses in [17] and has recently been observed experimentally in [18].

A large number of constitutive models, able to describe many features of the complex response of SMA, are available in the scientific literature [33, 23, 22, 8, 9] but most of them cannot model the occurrence of localized phase transformations. However, over the years, various different approaches have been used to describe the localizations in SMA.

The first attempts to model this phenomenology go back to [43] where FEM analyses based on standard 3-dimensional plasticity models were carried out to model the loading phase of SMA strips, later extended to take into account the thermomechanical coupling [42]. In [44, 10] a 1-dimensional nonlocal model for SMA bars based on two internal variables and a free energy depending on the strain gradient was proposed. Numerical simulations showed the ability of the model to describe the localized responses in tensile tests of SMA

wires. Another approach based on a series-asymptotic expansion method originating from the work [12] led to interesting analytical results in the study of phase transformations and the instability of SMA circular cylindrical wires [48, 47]. Implicit nonlocal gradient models were proposed in [14, 3] through the introduction of an internal length parameter that determines the nonlocality of the model through a partial differential equation. The model was then implemented in FEM codes and numerical results showed a good agreement with the experiments.

In this work, the study of the localization phenomena in pseudoelastic SMA bars, arising in tensile tests under displacement control, is addressed by using a variational approach within the framework of a global energetic formulation for rate-independent dissipative materials modeled by the constitutive specification of a free energy and a dissipation function [30, 29].

The evolution problem is stated by means of three energetic requirements: two of them reflect the first and second law of thermodynamics, the third one is a directional stability condition based on the minimization of the energy injection that would be needed to realize virtual radial continuation processes from a given state. The latter plays a role analogous to other criteria that provide restrictions on the dissipative behavior (like e.g. in [19, 25, 52]) but it offers the possibility to be interpreted in terms of stability as done, from slightly different perspectives in the important works [15, 35, 31]. Moreover, the approach is amenable to a robust numerical implementation by means of Incremental Energy Minimization [34] that will be discussed in forthcoming works.

The energetic criteria are stated in a global spatial and temporal form as proposed by Mielke and coworkers to obtain a derivative-free formulation able to deal with very weak smoothness requirements [30, 29]. The present analysis is however carried out without taking full advantage of the generality in [30] working instead with differential stability conditions in the spirit of Marigo and coworkers who successfully applied this type of criteria to the study of gradient damage models [36, 37, 38] and coupled damage and plasticity models [1, 2]. An application of this approach to SMA has recently appeared in [24] on the basis of a rather specific model. Moreover, with respect to [24], here the complete stability analysis of both homogeneous and non-homogeneous response is discussed.

The energetic formulation is described in Section 2 with reference to isothermal conditions which are a good approximation of the actual behavior only for very slow loading rates. This choice is done as the main motivation of the work is to show the applicability of the energetic approach in the most basic setting. The extension of the formulation to a full non-isothermal setting that properly takes into account the very important influence of the thermomechanical coupling is presently under development.

Section 2 also shows how the combined use of first-order directional stability and energy balance yields transformation criteria and kinetics both in variational and strong form. The discussion is referred to a class of SMA models characterized by the free energy functions proposed in [5, 6] modified by the introduction of a nonlocal term proportional to the gradient of the martensite fraction. The constitutive information is then completed by a positively homogeneous dissipation function as in [39, 7]. In this framework, various SMA models

with different levels of detail can be studied by using specific expressions for the effective elastic moduli, interaction energy and driving force thresholds as a function of the martensite fraction.

The attention is then restricted to the simplest version of the model specified by a constant elastic modulus, quadratic interaction energy and constant driving force thresholds, as described in Section 3. The consideration of more elaborate versions of the model, taking into account heterogeneity of the elastic properties of the phases, micromechanically derived interaction energies, non-constant driving force thresholds as well as tension-compression asymmetry, will be considered in forthcoming works.

In Section 4 the spatially homogeneous solutions are studied. Since the adopted free energy is non-convex in the internal variables, homogeneous phase transformations are accompanied by softening. The study of their stability then reveals that such solutions become unstable when the length of the bar exceeds an internal length ℓ_s determined by the dependence of the free energy density on the gradient of the phase fraction.

Given the instability of the homogeneous transformations, localized martensite fraction profiles may develop, provided that the length of the bar L is greater than a second internal length ℓ ($< \ell_s$), corresponding to the support of a half-localization. Due to the nonlocality of the model, the transformation criteria turn out to be to integro-differential equations that can be solved with the stress as a parameter. The stress is then computed from the knowledge of the average value of the martensite fraction. Section 5 and Appendix A discuss general properties of localized phase fraction profiles offering closed form expressions for the basic cases of boundary and inner localizations.

Section 6 discusses in detail the response of the bar when a single localization nucleates at the fixed end, grows and then propagates towards the other end. Explicit expressions are given for the nucleation and propagation stresses and it turns out that the corresponding stress drop is completely determined by the interaction energy and the local transformation strain. The analysis also shows that snap-back instabilities may occur depending on the length of the bar. More specifically, snap-back can occur if the bar is longer than the internal length ℓ_s of the material, during the phase of localization growth but also at the end of the transformation when the last untransformed region coalesces with the rest of the bar. In both cases, a stress drop is to be expected but it is shown that the one at the transformation completion must always be smaller than the one at the outset of the transformation. This helps to explain why the second type of stress drops are much more difficult to observe experimentally.

Section 7 provides some indications about the structure of localizations with multiple fronts and of their evolution that are easily handled in this framework. The occurrence of snap-back phenomena is discussed by introducing a third length L_s ($\geq \ell_s$), which depends not only on the internal length ℓ_s but also on the number of transformation fronts.

In section 8 the full stability analysis of the non-homogeneous solutions is carried out. The Rayleigh ratio associated with the second-variation of the difference between free energy and dissipation is studied explicitly, in closed form. The analysis shows that the localized transformation profiles are directionally stable provided the bar is sufficiently long to contain

at least the initial support of half localization and leaving room for some propagation, namely $L \geq \ell$. As result, for specific lengths L, such that $\ell \leq L < \ell_s$, both homogeneous and non-homogeneous solutions are admissible.

Finally, Section 9 offers the numerical simulation of a well known experiment [21]. The comparison shows a good agreement with the experiments in the simulation of the global response, especially in the Forward $A \to M$ Transformation. A good agreement is also obtained in the simulation of the spatio-temporal evolution of the transformation fronts.

Concerning notation, unless otherwise specified, the following will be assumed: the subscript t applied to a spatio-temporal field indicates the partial function at fixed time, like for example $f_t(x) := f(x,t)$; a prime indicates either the derivative with respect to the spatial coordinate or the directional derivative of functionals; a superposed dot means right-derivative with respect to time.

2. The Energetic Formulation of tensile tests under displacement control

The response of a SMA bar, of constant cross-section and subject to applied axial displacements (Figure 1), is studied by means of an energetic approach, based on the combined use of the laws of thermodynamics and a dissipative principle expressed in the form of a stability condition.

Attention is focused on the pseudoelastic behavior. Hence phase transformations are modeled, at each point x, by the evolution of a single martensite fraction $\alpha(x) \in [0,1]$ at temperatures above A_f, [11].

The *state* of the bar is described by three fields defined over the undeformed configuration $\Omega := [0, L]$ that represent displacement, temperature and phase fraction

$$(u, \alpha, T)$$

A *process* P for the bar is a time parametrized family of states

$$t \mapsto P_t := (u_t, \alpha_t, T_t), \qquad t \in [t_0, t_1]$$

Processes may be restricted to subintervals and, in the following, $P|_t$ will denote the process P restricted to $[t_0, t] \subseteq [t_0, t_1]$.

Except for Section 2.2, attention will be restricted to *isothermal* processes in which the temperature field is constant both in time and space, so that T will be considered as fixed parameter omitted from the list of state variables. The state space is thus $\mathcal{S} := \mathcal{U} \times \mathcal{V}$ where $\mathcal{U} := H^1([0,L], \mathbb{R})$ and $\mathcal{V} := H^2([0,L],[0,1])$ are the spaces to which displacement and phase fraction fields are assumed to belong, whereas processes are likewise assumed

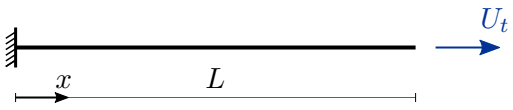

Figure 1: Tensile test setting.

to belong to $H^1([t_0,t_1],\mathcal{S})$. With such choices, gradients of fields and time derivatives of processes always exists, at least in a weak sense and the gradient of the phase fraction is continuous. Accordingly, even if not explicitly mentioned, most statements that involve the derivatives of the fields and of the processes holds almost everywhere in the respective domains of definition.

In the displacement controlled tensile test the left end ($x = 0$) of the bar is kept fixed while the right end ($x = L$) is subject to a given *loading history* U, namely a map

$$t \mapsto U_t, \qquad\qquad t \in [t_0, t_1]$$

in absence of body and surface forces. The loading is assumed to be smooth and slow enough to neglect inertia. This gives boundary conditions

$$u(0,t) = 0, \quad u(L,t) = U_t \tag{1}$$

The subset of kinematically admissible displacement fields (i.e. satisfying (1)) at time t, will be denoted $\mathcal{U}_{k,t} \subset \mathcal{U}$. On the contrary, no boundary conditions on the phase fractions are specified a priori while some natural ones will emerge from the following analysis. Initial conditions will correspond to the bar fully austenitic at a uniform temperature bigger than A_f, namely

$$u_0 = 0, \quad \alpha_0 = 0, \quad T_0 = \bar{T} > A_f$$

The isothermal test consists in a monotonic loading followed by a monotonic unloading described by

$$U_t := \begin{cases} Lt & \text{if } 0 \le t \le t_{\mathrm{u}} \\ -Lt + 2Lt_{\mathrm{u}} & \text{if } t_{\mathrm{u}} < t \le 2t_{\mathrm{u}} \end{cases} \tag{2}$$

which corresponds to the application of a displacement equal to the length of the bar in a unit of time. This choice of units helps to simplify notation and does not affect the results since the material behavior is assumed to be rate-independent.

2.1. Basic energetic quantities

The analysis is based on three quantities that specify how the bar stores and dissipates energy as well as how it exchanges energy with the environment.

The *Helmholtz free energy content* of the bar is given by

$$\mathcal{E}(u,\alpha,T) := \int_0^L \Phi\left(\varepsilon(x),\alpha(x),\gamma(x)\right) \mathrm{d}x \tag{3}$$

where Φ is a smooth constitutive function expressing free energy per unit length and $\varepsilon := u'$, $\gamma := \alpha'$ denote the axial strain and the gradient of the martensite fraction field. The dependence of the free energy density on γ will be, of course, crucial for the modeling of localizations. The stress at point x then reads

$$\sigma(x) := \frac{\partial \Phi}{\partial \varepsilon}\left(\varepsilon(x),\alpha(x),\gamma(x)\right) \tag{4}$$

The *dissipated power* corresponding to a martensite fraction profile α and a phase transformation field rate β, is defined as

$$D(\alpha, \beta) := \int_0^L \Gamma(\alpha(x), \beta(x)) \, \mathrm{d}x \tag{5}$$

where Γ is a constitutive function of the phase fraction and its rate that models the rate of energy dissipation per unit length. The dissipative evolution is assumed to be rate-independent, hence Γ is positively homogeneous of degree 1 in its second argument so that it turns out to be equivalent to a dissipation potential in the sense of the generalized standard materials, [19]. On the basis of (5), it is possible to compute the amount of *dissipated energy* in the bar for a given process P,

$$\mathcal{D}(P) := \int_{t_0}^{t_1} D(\alpha_\tau(x), \dot{\alpha}_\tau(x)) \, \mathrm{d}\tau \tag{6}$$

As temperature is constantly uniform, the *energy exchange with the environment* is purely mechanical due to the applied displacements at the boundary. The total energy supplied to the bar by the displacement history U, is

$$\mathcal{L}(U) := \int_{t_0}^{t_1} \left(\sigma_\tau(L) A \dot{U}_\tau \right) \mathrm{d}\tau \tag{7}$$

where $\sigma_\tau(L)$ is the stress at the moving end at time τ and A is the cross-section area.

2.2. The nonlocal constitutive model for SMA

According to (3) and (6), the constitutive behavior of the bar is completely determined by two scalar quantities: the free energy density Φ and the dissipation function Γ. This is consistent with the Ziegler-Green-Naghdi framework, used for SMA in [39] as well as in [7].

To deal with localizations of the phase transformations, a free energy density function consistent with the expressions proposed in [5] but augmented by a nonlocal term, quadratic in the gradient γ of the martensite fraction field is adopted

$$\begin{aligned} \Phi(\varepsilon, \alpha, \gamma, T) :=& \frac{1}{2} E(\alpha) (\varepsilon - \mu\alpha)^2 + B(T - T_e)\alpha + \\ &+ \Omega(\alpha)\alpha(1-\alpha) + \frac{1}{2} M \gamma^2 + \Phi_{ch}(T) \end{aligned} \tag{8}$$

where: $E(\alpha)$ is the elastic modulus, $\mu \geq 0$ the macroscopic transformation strain of the active type of martensite, T_e the equilibrium temperature at which pure austenite and martensite have the same free energy under stress-free conditions, $B \geq 0$ the entropy difference between the phases at equilibrium temperature T_e, $M \geq 0$ a parameter related to the internal length of the material and $\Phi_{ch}(T)$ the chemical free energy, [5].

The term containing the coefficient $\Omega(\alpha)$ is the interaction energy arising due to the incompatibility between the two phases at the microscopic scale and plays a crucial role

in SMA modeling. Several micromechanically-based expressions for it are available in the literature (see e.g. [5], [6], [33] and references therein). For what follows, it is important to remark that, as shown in [6], interaction energy has, in any case, to be bigger than the Reuss bound and smaller than the Voigt bound. This yields a constraint for the material parameters, namely

$$0 \leq \Omega(\alpha) < \frac{\mu^2 E(0)}{2} \tag{9}$$

that will be very important in the following. In the special case of constant Ω, interaction energy is non-negative for any value of the phase fraction and the free energy density is non-convex in α, except, of course, the limiting case of $\Omega = 0$, which is excluded from consideration.

The derivatives of the free energy density with respect to the martensite fraction and its gradient will have a key role and deserve a specific notation

$$\Pi_\alpha := -\frac{\partial \Phi}{\partial \alpha}, \qquad \Pi_\gamma := \frac{\partial \Phi}{\partial \gamma} \tag{10}$$

As it will be seen, the quantity

$$\Pi := \Pi_\alpha + \Pi'_\gamma \tag{11}$$

will play the role of *driving force of the phase transformations*. It is important to remark that it is given by the sum of a local part Π_α and a non-local part determined by the dependence of the free energy density Φ on the gradient of the phase fraction γ.

Concerning the second constitutive ingredient, it is assumed that the only dissipative phenomenon is the progress of the phase transformations and that the corresponding rate of energy dissipation is given by:

$$\Gamma\left(\alpha, \dot{\alpha}\right) := \Lambda_{\mathrm{F}}\left(\alpha\right) \dot{\alpha}^{+} + \Lambda_{\mathrm{R}}(\alpha) \dot{\alpha}^{-} \tag{12}$$

where $\dot{\alpha}^{+} := \max\left(\dot{\alpha}, 0\right)$ and $\dot{\alpha}^{-} := \min\left(\dot{\alpha}, 0\right)$. The constitutive functions $\Lambda_{\mathrm{F}}(\alpha)$ and $\Lambda_{\mathrm{R}}(\alpha)$ can be interpreted as the threshold levels that the driving force must reach in order to activate the phase transformations. In particular, their eventual explicit dependence on the phase fraction determines different slopes for the pseudoelastic plateaus. The thresholds are generally different for the two transformations and the subscripts F, R here and in the following denote respectively Forward Transformation (FwT) $A \to M$ (increasing α) and Reverse Transformation (RvT) $M \to A$ (decreasing α). With this choice, the dissipation function is convex, satisfies $\Gamma(\alpha, 0) = 0$ and is homogeneous of degree 1 with respect to the phase fraction rate.

2.3. Energetic requirements on processes

The *evolution problem* amounts to find the processes that the bar can undergo under a given displacement history. This will be stated by means of three energetic criteria.

> *A process P is* energetically consistent *with the environment if, for each $t \in [t_0, t_1]$, the following energy balance holds*
>
> $$\mathcal{E}_P(t) - \mathcal{E}_P(t_0) + \mathcal{D}_P(t) = \mathcal{L}_U(t) \tag{EB}$$

where $\mathcal{E}_P(t) := \mathcal{E}(P_t) = \mathcal{E}(u_t, \alpha_t)$ is the free energy evaluated along the process and $\mathcal{D}_P(t) := \mathcal{D}(P|_t)$ is the energy dissipated in the process $P|_t$ obtained by restriction of P on the subinterval $[t_0, t]$. Similarly $\mathcal{L}_U(t) := \mathcal{L}(U|_t)$ is the energy supplied by the applied displacements[1] U_t up to time t.

A process P is said to satisfy the irreversibility condition *if, for each $t \in [t_0, t_1]$, the rate of energy dissipation is non-negative at any point:*

$$\Gamma(\alpha_t(x), \dot{\alpha}_t(x)) \geq 0 \tag{IR}$$

In this context, with a slightly abuse of notation, both reversible and irreversible processes, for which respectively the rate of energy dissipation is vanishing or positive, are meant to satisfy (IR).
Taking into account the structure (12) of the dissipation function, the irreversibility condition is then automatically satisfied if the constitutive functions in (12) obey the following fundamental sign restrictions:

$$\Lambda_{\mathrm{F}}(\alpha) \geq 0, \quad \text{and} \quad \Lambda_{\mathrm{R}}(\alpha) \leq 0 \tag{13}$$

While energy balance and irreversibility are nothing but particular statements of the first and second law of thermodynamics, they are not enough to characterize the evolution of phase transformations and further restrictions are needed. While such restrictions can be implemented in various ways, [28, 34, 19, 52, 15, 27, 25], here a stability condition that involves the energetic comparison among different competing admissible states is used.

Due to the possibility of energy dissipation, the comparison between the energy of different states is, in general, process-dependent. If the competing states are allowed to vary over the whole state space this leads to the notion of global stability that requires variational statements over the whole space of processes. On the other hand, directional stability conditions involve comparisons over restricted subsets of competing states parameterizable in a way that can be usefully interpreted as a special kind of virtual continuation processes.

Specifically, a *radial continuation process* starting from the state (u, α) in the *test direction* $(\tilde{u}, \tilde{\alpha})$ is a map

$$\tau \mapsto (u + \tau\tilde{u},\ \alpha + \tau\tilde{\alpha}), \qquad \tau \in [0, h] \tag{14}$$

If τ is assumed to have the dimensions of time, the test directions have the dimensions of rates and must satisfy some conditions to ensure that all states reached by the continuation are admissible. In particular, in order to preserve displacement boundary conditions, displacement test directions must belong to

$$\mathcal{U}_0 := \{\tilde{u} \in \mathcal{U} \quad | \quad \tilde{u}(0) = \tilde{u}(L) = 0\} \tag{15}$$

[1] Of course, in presence of applied forces, energy exchanges with the environment will also have to take into account the potential energy of the loading device.

On the contrary, phase fraction fields are not constrained, a priori, by boundary conditions but, due to the fact that their values must belong to a bounded interval, there are state-dependent sign restrictions on the test direction fields that must belong to

$$\mathcal{V}_\alpha := \{\tilde{\alpha} \in \mathcal{V} \mid \tilde{\alpha}(x) \geq 0, \text{ if } \alpha(x) = 0 \quad \text{and} \quad \tilde{\alpha}(x) \leq 0, \text{ if } \alpha(x) = 1\} \tag{16}$$

This simply means that, at every point of pure austenite, test directions for the phase fraction cannot be negative, while at points of pure martensite test directions cannot be positive.

For coming mathematical manipulations it is also useful to introduce the test directions

$$\mathcal{V}_\alpha^+ := \mathcal{V}_\alpha \cap \{\tilde{\alpha} \in \mathcal{V} \mid \tilde{\alpha} \geq 0\}, \qquad \mathcal{V}_\alpha^- := \mathcal{V}_\alpha \cap \{\tilde{\alpha} \in \mathcal{V} \mid \tilde{\alpha} \leq 0\} \tag{17}$$

A process P is directionally stable *at time $t \in [t_0, t_1]$ if there exists a continuation interval $[0, \bar{h}]$ such that the free energy change induced by any radial continuation process starting from $P_t = (u_t, \alpha_t)$ does not exceed the corresponding energy dissipation, namely for every $h \in [0, \bar{h}]$, it must be*

$$\mathcal{E}(u_t + h\tilde{u}, \alpha_t + h\tilde{\alpha}) - \mathcal{E}(u_t, \alpha_t) + \mathcal{D}_h(\alpha_t, \tilde{\alpha}) \geq 0, \quad \forall (\tilde{u}, \tilde{\alpha}) \in \mathcal{U}_0 \times \mathcal{V}_{\alpha_t} \tag{DS}$$

In (DS), $\mathcal{D}_h(\alpha_t, \tilde{\alpha})$ is the energy dissipated in the radial continuation process determined by the direction $\tilde{\alpha}$ from the state α_t, during the continuation interval $[0, h]$. By (EB) the sum of the free energy change and the energy dissipated during a process is equal to the energy supply from the environment, hence the left-hand side in (DS) can be interpreted as the energy injection from the exterior that would be needed in order to sustain the virtual radial continuation process. In this way, directional stability can be interpreted as the requirement that actual states correspond to local minima of the energy injection.

In this framework the *evolution problem* consists in finding the processes P that satisfy the three energetic criteria (EB), (IR), (DS) for a given environment specified by a displacement history U.

As it will be seen, this naturally leads to the study of the material stability and therefore is particularly useful in the study of localization phenomena. Moreover it is amenable to robust numerical implementation via incremental energy minimization.

2.4. Derivatives of the energetic quantities

In the next sections repeated use of various derivatives of the energetic quantities will be made, hence it is useful to record here the general expressions that will be used.

The first directional derivative of the free energy (3) at the state (u, α) evaluated in the direction $(\tilde{u}, \tilde{\alpha})$ will be denoted $\mathcal{E}'(u, \alpha; \tilde{u}, \tilde{\alpha})$ and, under the adopted constitutive assumptions, turns out to be continuous in the state hence linear with respect to the directions, so that

$$\mathcal{E}'(u, \alpha; \tilde{u}, \tilde{\alpha}) = \mathcal{E}'(u, \alpha; \tilde{u}, 0) + \mathcal{E}'(u, \alpha; 0, \tilde{\alpha}) \tag{18}$$

Denoting $\tilde{\varepsilon} := \tilde{u}'$, $\tilde{\gamma} := \tilde{\alpha}'$ and taking into account (8) and (12) as well as the definitions of the stress (4) and of the driving forces (10)

$$\mathcal{E}'\left(u, \alpha; \tilde{u}, 0\right) = \int_0^L \left(\sigma\tilde{\varepsilon}\right) \mathrm{d}x \tag{19}$$

$$\mathcal{E}'\left(u, \alpha; 0, \tilde{\alpha}\right) = \int_0^L \left(-\Pi_\alpha\tilde{\alpha} + \Pi_\gamma\tilde{\gamma}\right) \mathrm{d}x \tag{20}$$

Similarly, the second directional derivative of the free energy (3) at the state (u, α) evaluated in the directions $(\tilde{u}_1, \tilde{\alpha}_1)$ and $(\tilde{u}_2, \tilde{\alpha}_2)$ can be written, taking into account (8), as

$$\begin{aligned}\mathcal{E}''\left(u, \alpha; \tilde{u}_1, \tilde{\alpha}_1; \tilde{u}_2, \tilde{\alpha}_2\right) = &\int_0^L \left(\frac{\partial\sigma}{\partial\varepsilon}\tilde{\varepsilon}_1\tilde{\varepsilon}_2 - \frac{\partial\Pi_\alpha}{\partial\alpha}\tilde{\alpha}_1\tilde{\alpha}_2 + \frac{\partial\Pi_\gamma}{\partial\gamma}\tilde{\gamma}_1\tilde{\gamma}_2\right) \mathrm{d}x + \\ &+ \int_0^L \left(\frac{\partial\sigma}{\partial\alpha}\tilde{\varepsilon}_1\tilde{\alpha}_2 - \frac{\partial\Pi_\alpha}{\partial\varepsilon}\tilde{\alpha}_1\tilde{\varepsilon}_2\right) \mathrm{d}x\end{aligned} \tag{21}$$

The directional derivative of the dissipated power (5) with respect to its first argument in the direction $\tilde{\alpha}$ is given by

$$D'(\alpha, \beta; \tilde{\alpha}) = \int_0^L \left(\frac{\partial\Lambda_{\mathrm{F}}}{\partial\alpha}\beta^+ + \frac{\partial\Lambda_{\mathrm{R}}}{\partial\alpha}\beta^-\right)\tilde{\alpha}\,\mathrm{d}x \tag{22}$$

The first and second derivatives of the energy $\mathcal{D}_h(\alpha, \tilde{\alpha})$ dissipated in the radial continuation from the state (u, α) in the direction $(\tilde{u}, \tilde{\alpha})$ of duration h, with respect to h at $h = 0$ and fixed direction will also be needed. Taking into account (6), (5) and (12) it turns out that

$$\mathcal{D}_0'\left(\alpha, \tilde{\alpha}\right) = D(\alpha, \tilde{\alpha}) = \int_0^L \left(\Lambda_{\mathrm{F}}\tilde{\alpha}^+ + \Lambda_{\mathrm{R}}\tilde{\alpha}^-\right) \mathrm{d}x \tag{23}$$

$$\mathcal{D}_0''\left(\alpha, \tilde{\alpha}\right) = D'(\alpha, \tilde{\alpha}; \tilde{\alpha}) = \int_0^L \left(\frac{\partial\Lambda_{\mathrm{F}}}{\partial\alpha}\tilde{\alpha}^+ + \frac{\partial\Lambda_{\mathrm{R}}}{\partial\alpha}\tilde{\alpha}^-\right)\tilde{\alpha}\ \mathrm{d}x \tag{24}$$

2.5. Differential directional stability

Whenever the energetic quantities possess enough directional derivatives it is possible to expand in series the left-hand side of (DS), as in [38], and hence to adopt a general strategy to enforce the stability condition (DS) based on a sequence of necessary and sufficient conditions obtained by restricting the energetic comparisons to processes of infinitesimal duration of increasing order.

A process P is directionally stable at the first order *if, for any time $t \in [t_0, t_1]$,*

$$\mathcal{E}'\left(u_t, \alpha_t; \tilde{u}, \tilde{\alpha}\right) + \mathcal{D}_0'(\alpha_t, \tilde{\alpha}) \geq 0 \qquad \forall(\tilde{u}, \tilde{\alpha}) \in \mathcal{U}_0 \times \mathcal{V}_{\alpha_t} \tag{DS1}$$

for any admissible test direction $(\tilde{u}, \tilde{\alpha})$ from the state $P_t = (u_t, \alpha_t)$.

Taking into account (18), (19), (20) and (23) this can be written

$$\int_0^L (\sigma\,\tilde{\varepsilon})_t\,\mathrm{d}x + \int_0^L \left(-\Pi_\alpha\,\tilde{\alpha} + \Pi_\gamma\,\tilde{\gamma} + \Lambda_{\mathrm{F}}\tilde{\alpha}^+ + \Lambda_{\mathrm{R}}\tilde{\alpha}^-\right)_t \mathrm{d}x \geq 0 \qquad \forall(\tilde{u},\tilde{\alpha}) \in \mathcal{U}_0 \times \mathcal{V}_{\alpha_t} \quad (25)$$

where the subscript t, here and henceforth, indicates that all the state-dependent quantities included within the parentheses are evaluated at the given process at time t.

The fulfillment of (DS1) is a necessary but not sufficient condition for the validity of the directional stability (DS). In general, if the state satisfies first-order stability, there is a set of directions for which it holds as an equality

$$\mathcal{S}_1(u_t,\alpha_t) := \{(\tilde{u},\tilde{\alpha}) \in \mathcal{U}_0 \times \mathcal{V}_{\alpha_t} \Rightarrow \mathcal{E}'\,(u_t,\alpha_t;\tilde{u},\tilde{\alpha}) + \mathcal{D}_0'\,(\alpha_t,\tilde{\alpha}) = 0\} \quad (26)$$

and the complementary set of directions for which it holds as a strict inequality

$$\mathcal{S}_2(u_t,\alpha_t) := \{(\tilde{u},\tilde{\alpha}) \in \mathcal{U}_0 \times \mathcal{V}_{\alpha_t} \Rightarrow \mathcal{E}'\,(u_t,\alpha_t;\tilde{u},\tilde{\alpha}) + \mathcal{D}_0'\,(\alpha_t,\tilde{\alpha}) > 0\}$$

If $\mathcal{S}_2 = \mathcal{U}_0 \times \mathcal{V}_{\alpha_t}$, namely the condition is satisfied as an inequality for all test directions, (DS1) is also sufficient for full stability. Otherwise it becomes necessary to analyze the second-order stability relatively to the set $\mathcal{S}_1$ of directions for which (DS1) is satisfied as an equality.

> *A process P is* directionally stable at the second order *if for any time $t \in [t_0,t_1]$ either first-order stability is satisfied as a strict inequality for all directions $(\tilde{u},\tilde{\alpha})$ from the state $P_t = (u_t,\alpha_t)$, namely $\mathcal{S}_2(u_t,\alpha_t) = \mathcal{U}_0 \times \mathcal{V}_{\alpha_t}$, or*
>
> $$\mathcal{E}''(u_t,\alpha_t;\tilde{u},\tilde{\alpha};\tilde{u},\tilde{\alpha}) + \mathcal{D}_0''(\alpha_t,\tilde{\alpha}) \geq 0 \qquad \forall(\tilde{u},\tilde{\alpha}) \in \mathcal{S}_1(u_t,\alpha_t) \qquad \text{(DS2)}$$

Taking into account (21) and (25), the inequality in (DS2) can be written as

$$\int_0^L \left(\frac{\partial\sigma}{\partial\varepsilon}\tilde{\varepsilon}^2 - \frac{\partial\Pi_\alpha}{\partial\alpha}\tilde{\alpha}^2 + \frac{\partial\Pi_\gamma}{\partial\gamma}\tilde{\gamma}^2 - 2\frac{\partial\Pi_\alpha}{\partial\varepsilon}\tilde{\varepsilon}\tilde{\alpha} + \frac{\partial\Lambda_{\mathrm{F}}}{\partial\alpha}\tilde{\alpha}^+ + \frac{\partial\Lambda_{\mathrm{R}}}{\partial\alpha}\tilde{\alpha}^-\right)_t \mathrm{d}x \geq 0 \qquad \forall(\tilde{u},\tilde{\alpha}) \quad (27)$$

The fulfillment of (DS2) is another necessary condition for the validity of (DS) that becomes sufficient if it is satisfied as a strict inequality for directions $\mathcal{S}_1$. If the sufficient condition is not yet attained the procedure can be iterated by enforcing stability of higher orders, but hereinafter this will be never necessary.

Combining the above results, a sufficient condition for the validity of full directional stability, that makes sense provided the energetic quantities possess enough directional differentiability, is obtained :

> *A process is* directionally stable *if for any time $t \in [t_0,t_1]$ there in an integer $n > 0$ such that*
>
> $$\mathcal{E}^{(n)}(u_t,\alpha_t;\tilde{u},\tilde{\alpha}) + \mathcal{D}_0^{(n)}(\alpha_t,\tilde{\alpha}) > 0 \quad \forall(\tilde{u},\tilde{\alpha}) \in \mathcal{S}_{(n-1)}(u_t,\alpha_t) \qquad (28)$$

and moreover, if $n > 1$,

$$\mathcal{E}^{(k)}(u_t, \alpha_t; \tilde{u}, \tilde{\alpha}) + \mathcal{D}_0^{(k)}(\alpha_t, \tilde{\alpha}) \geq 0 \quad \forall (\tilde{u}, \tilde{\alpha}) \in \mathcal{S}_{(k-1)}(u_t, \alpha_t) \quad k = 1, \dots, n-1 \tag{29}$$

where the subsets of directions to be tested at each order are given by

$$\mathcal{S}_k(u_t, \alpha_t) := \left\{ (\tilde{u}, \tilde{\alpha}) \in \mathcal{U}_0 \times \mathcal{V}_{\alpha_t} \quad | \quad \mathcal{E}^{(k)}(u_t, \alpha_t; \tilde{u}, \tilde{\alpha}) + \mathcal{D}_0^{(k)}(\alpha_t, \tilde{\alpha}) = 0 \right\}$$
$$\mathcal{S}_0(u_t, \alpha_t) := \mathcal{U}_0 \times \mathcal{V}_{\alpha_t}$$

This is a sufficient condition which, however, is not necessary and in fact there is another possibility for full stability to hold.

A process is indefinitely stable *if for any time* $t \in [t_0, t_1]$ *and* any *integer* $k > 0$ *the set* $\mathcal{S}_k(u_t, \alpha_t)$ *is non empty and*

$$\mathcal{E}^{(k)}(u_t, \alpha_t; \tilde{u}, \tilde{\alpha}) + \mathcal{D}_0^{(k)}(\alpha_t, \tilde{\alpha}) \geq 0 \quad \forall (\tilde{u}, \tilde{\alpha}) \in \mathcal{S}_{(k-1)}(u_t, \alpha_t) \tag{30}$$

An indefinitely stable process does satisfy the full (DS) and it is the analogue of indifferent equilibrium in classical elastic stability.

2.6. Solution strategy

Once the energetic quantities have been made explicit, the characterization of the processes that solve the evolution problem can be carried out by the following two-steps strategy.

Responses consistent with first-order directional stability (DS1) and energy balance (EB), as well as irreversibility (IR) are determined first and called *candidate solutions*. This is possible since, as it will be shown, the combined use of first-order stability and energy balance leads to the statement of phase transformation criteria and phase transformation kinetics that can be solved to determine the corresponding processes. Moreover, as discussed above, the irreversibility condition can be taken into account, automatically, by enforcing sign restrictions (13) on the constitutive prescription of the driving force thresholds, that will be systematically assumed to hold.

Afterwards, since first-order stability is a necessary condition for directional stability, candidate solutions are tested by checking, a posteriori, the second-order stability condition for the fulfillment of the full directional stability (DS).

In view of the following discussion it is useful to introduce a further piece of notation. A phase fraction field α induces a partition of the bar into three disjoint subdomains composed by points that are either pure phases or a mixture of the two. Similarly, a field of rates $\dot{\alpha}$ induces another partition of the bar into three disjoint subdomains of transforming and non transforming points.

$$\begin{aligned} S_{\mathrm{A}}(\alpha) &:= \{x \in \Omega \,|\, \alpha(x) = 0\} & FwT(\dot{\alpha}) &:= \{x \in \Omega \,|\, \dot{\alpha}(x) > 0\} \\ S_{\mathrm{M}}(\alpha) &:= \{x \in \Omega \,|\, \alpha(x) = 1\} & RvT(\dot{\alpha}) &:= \{x \in \Omega \,|\, \dot{\alpha}(x) < 0\} \\ S_{\mathrm{AM}}(\alpha) &:= \{x \in \Omega \,|\, 0 < \alpha(x) < 1\} & NoT(\dot{\alpha}) &:= \{x \in \Omega \,|\, \dot{\alpha}(x) = 0\} \end{aligned} \tag{31}$$

Of course, for any pair of fields α and $\dot{\alpha}$ the following relations have to hold:

$$FwT \subseteq S_{\mathrm{A}} \cup S_{\mathrm{AM}}, \qquad RvT \subseteq S_{\mathrm{M}} \cup S_{\mathrm{AM}} \tag{32}$$

2.7. Transformation criteria as a consequence of first-order stability

To analyze the consequences of first-order differential directional stability, the terms containing $\tilde{u}'$ and $\tilde{\alpha}'$ can be eliminated from (25) after integration by parts. Using the definitions (10), (11) of the driving force Π as well as (12) and (15), the first-order directional stability becomes:

$$\int_0^L \left(-\sigma'\tilde{u} - \Pi\tilde{\alpha} + \Lambda_F\tilde{\alpha}^+ + \Lambda_{\mathrm{R}}\tilde{\alpha}^-\right)_t \mathrm{d}x + \left[\left(\Pi_\gamma\right)_t \tilde{\alpha}\right]_0^L \geq 0 \qquad \forall\,(\tilde{u},\tilde{\alpha}) \in \mathcal{U}_0 \times \mathcal{V}_\alpha \tag{33}$$

Further consequences can now be determined by standard arguments of the calculus of variations, considering suitable special cases of test directions.

Continuations at fixed phase fraction ($\tilde{\alpha} = 0$) and arbitrary admissible $\tilde{u}$ together with the continuity of σ over $[0, L]$ yield global and local mechanical equilibrium equations:

$$-\int_0^L \left(\sigma'\right)_t \tilde{u}\,\mathrm{d}x \geq 0 \quad \forall\tilde{u} \in \mathcal{U}_0 \quad \rightarrow \quad \sigma_t(x) = f(t) \tag{34}$$

namely the stress field is spatially uniform at any time t. This also means that first-order stability is necessarily satisfied as an equality for all continuations at fixed phase fraction, namely

$$\mathcal{E}'(u_t, \alpha_t; \tilde{u}, 0) = 0 \qquad \forall\tilde{u} \in \mathcal{U}_0 \tag{35}$$

Continuations at fixed displacement ($\tilde{u} = 0$) with arbitrary positive phase fraction null at the boundary yield

$$\int_{S_{\mathrm{A}}\cup S_{\mathrm{AM}}} \left(-\Pi + \Lambda_{\mathrm{F}}\right)_t \tilde{\alpha}\,\mathrm{d}x \geq 0 \qquad \forall\tilde{\alpha} \in \left\{\mathcal{V}_\alpha^+ \mid \tilde{\alpha}(0) = \tilde{\alpha}(L) = 0\right\} \tag{36}$$

since $\tilde{\alpha}(x) = 0$ in S_{M}. Similarly, continuations at fixed displacement ($\tilde{u} = 0$) with arbitrary negative phase fraction null at the boundary yield

$$\int_{S_{\mathrm{M}}\cup S_{\mathrm{AM}}} \left(-\Pi + \Lambda_{\mathrm{R}}\right)_t \tilde{\alpha}\,\mathrm{d}x \geq 0 \qquad \forall\tilde{\alpha} \in \left\{\mathcal{V}_\alpha^- \mid \tilde{\alpha}(0) = \tilde{\alpha}(L) + = 0\right\} \tag{37}$$

since $\tilde{\alpha}(x) = 0$ in S_{A}.

As it will be seen, the two conditions (36) and (37) derived from the first-order directional stability (DS1) can be interpreted as variational formulation of phase transformation criteria. When integrands are continuous, arbitrariness of the test directions yield, at any time (omitting from the notation the dependence from t)

$$\Pi(x) \leq \Lambda_{\mathrm{F}}(x) \qquad \text{if} \quad x \in S_{\mathrm{A}} \tag{38}$$

$$\Lambda_{\mathrm{R}}(x) \leq \Pi(x) \leq \Lambda_{\mathrm{F}}(x) \qquad \text{if} \quad x \in S_{\mathrm{AM}} \tag{39}$$

$$\Pi(x) \geq \Lambda_{\mathrm{R}}(x) \qquad \text{if} \quad x \in S_{\mathrm{M}} \tag{40}$$

This provides *phase transformation criteria* in terms of the driving force (11). As it will be discussed in detail, due to the presence of the gradient of the phase fraction in the free

energy density (8) the resulting criteria are nonlocal and this will be crucial in the study of localizations. Transformation criteria show that the driving force cannot exceed the threshold $\Lambda_{\rm F}$ unless it is in pure martensite nor it can be less than $\Lambda_{\rm R}$ unless it is pure austenite.

Again by standard variational arguments that involve the consideration of suitable sequences of test directions (with $\tilde{u} = 0$) and taking into account (8), the first-order stability, (DS1) reduces to

$$M\left[\alpha_t'\left(L\right)\tilde{\alpha}\left(L\right)\right] \geq 0, \qquad -M\left[\alpha_t'\left(0\right)\tilde{\alpha}\left(0\right)\right] \geq 0 \qquad \forall \tilde{\alpha}(0), \tilde{\alpha}(L) \in \mathcal{V}_\alpha\left(\{0, L\}\right) \tag{41}$$

Since $M \geq 0$, the state-dependent sign restrictions (16) on $\tilde{\alpha}$ and the continuity of α_t' yield the following boundary conditions for the gradient of the phase fraction

$$\alpha_t'(0) = 0, \qquad \alpha_t'(L) = 0 \tag{42}$$

In order to understand (36, 37), or their counterparts (38-40), as phase transformation criteria, it is necessary to study the consequences of the energy balance. For this purpose it is enough to consider it with respect to each subprocess of infinitesimal duration.

A process P is energetically consistent with the environment at the first order *if for any time $t \in [t_0, t_1]$ the following power balance holds*

$$\dot{\mathcal{E}}_P(t) + \dot{\mathcal{D}}_P(t) = \dot{\mathcal{L}}_U(t) \tag{43}$$

This involves the right-derivatives of the functions of time that enter in (EB). Provided that the energetic quantities are sufficiently regular, (43) is sufficient for the validity of energy balance. It turns out that $\dot{\mathcal{E}}_P(t) = \mathcal{E}'(u_t, \alpha_t; \dot{u}_t, \dot{\alpha}_t)$ and that $\dot{\mathcal{D}}_P(t) = \mathcal{D}_0'(\alpha_t, \dot{\alpha}_t)$ therefore the left-hand side of (43) is equal to the corresponding term in the first-order directional stability (DS1) evaluated with test directions equal to the actual rates in the process. Moreover, using (7) and the linearity of $\mathcal{E}'$ in the test directions, the balance (43) can be written as:

$$\mathcal{E}'\left(u_t, \alpha_t; \dot{u}_t, 0\right) + \mathcal{E}'\left(u_t, \alpha_t; 0, \dot{\alpha}_t\right) + \mathcal{D}_0'\left(\alpha_t, \dot{\alpha}_t\right) = \sigma_t(L)\, A\, \dot{U}_t \tag{44}$$

However (34) and (1) imply that $\mathcal{E}'\left(u_t, \alpha_t; \dot{u}_t, 0\right) = \dot{\mathcal{L}}_U(t)$ hence (44) yields the following reduced first-order energy balance

$$\mathcal{E}'\left(u_t, \alpha_t; 0, \dot{\alpha}_t\right) + \mathcal{D}_0'\left(\alpha_t, \dot{\alpha}_t\right) = 0 \tag{45}$$

that, after integration by parts with respect to $\tilde{\alpha}'$ in (25) and consideration of (42), explicitly reads

$$\int_0^L \left(-\Pi\, \dot{\alpha} + \Lambda_{\rm F}\, \dot{\alpha}^+ + \Lambda_{\rm R}\, \dot{\alpha}^-\right)_t \mathrm{d}x = 0 \tag{46}$$

This plays the role of a dissipative balance between the power released and dissipated during the actual process of phase transformations. Using the partition (31) induced by the field of rates $\dot{\alpha}_t$, (46) reduces to:

$$\int_{FwT_t} \left(\left(-\Pi + \Lambda_{\rm F}\right)\dot{\alpha}\right)_t \, \mathrm{d}x + \int_{RvT_t} \left(\left(-\Pi + \Lambda_{\rm R}\right)\dot{\alpha}\right)_t \, \mathrm{d}x = 0 \tag{47}$$

Taking into account (32) and the transformation criteria (38-40) obtained as consequences of the first-order directional stability, it turns out that the left-hand side of (47) is the sum of two non-negative quantities hence the two integrands must both be zero. Since this has to hold for any admissible rate it follows that, at any point where the integrands of (47) are continuous

$$(-\Pi + \Lambda_{\mathrm{F}})\dot{\alpha}^{+} = 0, \qquad \text{in } FwT \tag{48}$$

$$(-\Pi + \Lambda_{\mathrm{R}})\dot{\alpha}^{-} = 0, \qquad \text{in } RvT \tag{49}$$

where the dependence on t has been omitted. More explicitly, (48) and (49) equals to

$$\begin{array}{lll} \dot{\alpha}(x) > 0 & \rightarrow & \Pi(x) = \Lambda_{\mathrm{F}}(x) \\ \dot{\alpha}(x) < 0 & \rightarrow & \Pi(x) = \Lambda_{\mathrm{R}}(x) \end{array} \tag{50}$$

This means that the occurrence of the phase transformations is possible only if the driving force Π, defined in (11), is equal to the quantities that characterize the dissipation function (12). Accordingly, $\Lambda_{\mathrm{F,R}}$ can be interpreted as a model for the resistance that need to be overcome in order to activate the phase transformations.

Therefore, at each time, the bar is partitioned into the set of points where transformation criteria are satisfied as an equality

$$\overline{FwT} := \{x \in [0, L] \quad | \quad \Pi(x) = \Lambda_{\mathrm{F}}(x), \quad 0 \leq \alpha(x) < 1\} \supseteq FwT \tag{51}$$

$$\overline{RvT} := \{x \in [0, L] \quad | \quad \Pi(x) = \Lambda_{\mathrm{R}}(x), \quad 0 < \alpha(x) \leq 1\} \supseteq RvT \tag{52}$$

that include the transforming regions, and the remaining part where the transformation criteria are satisfied as strict inequalities and transformation cannot occur.

2.8. Transformation kinetics

The evolution of the phase transformations, can be described through a kinetic equation that can be obtained by enforcing the first-order stability (DS1) and first-order energy balance (43) at infinitesimally close instants. To this end, note that, by (34) and (42), the first order stability (DS1) at time $t + \tau$ can be written as

$$\mathcal{E}'\left(u_{t+\tau}, \alpha_{t+\tau}; 0, \tilde{\alpha}\right) + \mathcal{D}_0'\left(\alpha_{t+\tau}, \tilde{\alpha}\right) =: g(\tau, \tilde{\alpha}) \geq 0 \quad \forall \tilde{\alpha} \text{ and } \forall \tau > 0 \tag{53}$$

whence, in particular, $g\left(0, \tilde{\alpha}\right) \geq 0$. Moreover, the reduced energy balance (45) yields $g\left(0, \dot{\alpha}_t\right) = 0$, then evaluating the left and right derivatives with respect to τ at $\tau = 0$ and invoking the Nguyen continuity argument [32] it follows that:

$$\dot{g}(0, \dot{\alpha}_t) = 0$$

More explicitly, this means that

$$\mathcal{E}''\left(u_t, \alpha_t; \dot{u}, \dot{\alpha}; 0, \dot{\alpha}\right) + D'\left(\alpha_t, \dot{\alpha}_t; \dot{\alpha}_t\right) = 0 \tag{54}$$

By arguments similar to those used to derive (48) and (49) the consistency condition (54) implies

$$\int_{FwT} \left(-\dot{\Pi} + \dot{\Lambda}_F\right)_t \dot{\alpha}_t \, \mathrm{d}x = 0 \qquad \int_{RvT} \left(-\dot{\Pi} + \dot{\Lambda}_R\right)_t \dot{\alpha}_t \, \mathrm{d}x = 0 \tag{55}$$

that are global statements of the transformation kinetics for the two phase transformations.

2.9. Characterization of candidate solutions

Putting together transformation criteria (48) and (49) and transformation kinetics (55) it follows that candidate solutions are characterized, at any time and at any point where the driving force and the phase fraction rates are continuous, by the following constraints:

- at any point of pure austenite ($\alpha(x) = 0$) :

$$\begin{array}{lll} \Pi(x) < \Lambda_{\mathrm{F}}(x) & \rightarrow & \dot{\alpha}(x) = 0 \\ \dot{\alpha}(x) > 0 & \rightarrow & \Pi(x) = \Lambda_{\mathrm{F}}(x) \quad \text{and} \quad \dot{\Pi}(x) = \dot{\Lambda}_F(x) \end{array} \tag{56}$$

- at any point of mixture ($0 < \alpha(x) < 1$):

$$\begin{array}{lll} \Lambda_{\mathrm{R}}(x) < \Pi(x) < \Lambda_{\mathrm{F}}(x) & \rightarrow & \dot{\alpha}(x) = 0 \\ \dot{\alpha}(x) > 0 & \rightarrow & \Pi(x) = \Lambda_{\mathrm{F}}(x) \quad \text{and} \quad \dot{\Pi}(x) = \dot{\Lambda}_F(x) \\ \dot{\alpha}(x) < 0 & \rightarrow & \Pi(x) = \Lambda_{\mathrm{R}}(x) \quad \text{and} \quad \dot{\Pi}(x) = \dot{\Lambda}_R(x) \end{array} \tag{57}$$

- at any point in pure martensite ($\alpha(x) = 1$);

$$\begin{array}{lll} \Pi(x) > \Lambda_{\mathrm{R}}(x) & \rightarrow & \dot{\alpha}(x) = 0 \\ \dot{\alpha}(x) < 0 & \rightarrow & \Pi(x) = \Lambda_{\mathrm{R}}(x) \quad \text{and} \quad \dot{\Pi}(x) = \dot{\Lambda}_R(x) \end{array} \tag{58}$$

The search of candidate solutions will be carried out by first computing phase fraction fields satisfying transformation criteria in the form $\Pi = \Lambda$ and then checking if and how they can evolve according to $\dot{\Pi} = \dot{\Lambda}$.

The issue of the uniqueness of processes satisfying the above requirements can be discussed by a bifurcation analysis that, in this context, can be carried out by stating the global consistency condition (54) as a variational inequality. This follows by subtracting the reduced energy balance equality $\dot{g}(0, \dot{\alpha}) = 0$ from the inequality $\dot{g}(0, \tilde{\alpha}) \geq 0$ obtained as time derivative of first-order directional stability:

$$\mathcal{E}''\left(u_t, \alpha_t; \dot{u}_t, \dot{\alpha}_t, 0, \tilde{\alpha} - \dot{\alpha}_t\right) + D'\left(\alpha_t, \tilde{\alpha}; \dot{\alpha}_t\right) - D'\left(\alpha_t, \dot{\alpha}_t; \dot{\alpha}_t\right) \geq 0, \quad \forall \tilde{\alpha}$$

The detailed bifurcation analysis is beyond the scopes of this work that, on the other hand, will be focused on the comparison between spatially homogeneous and non-homogeneous candidate solutions.

2.10. Stability analysis

The final stability analysis consists in the check of the sufficient conditions of (DS1) and (DS2) for full stability over all processes that solve transformation kinetics and criteria, namely that satisfy (56-58). This consists in the verification of the validity of (27), a task that may be strongly dependent on the particular constitutive model at hand. For some models its analytical evaluation may become prohibitive and the recourse to numerical analysis is unavoidable. On the contrary, in the following, the attention will be restricted to a special constitutive model for which the complete stability analysis can be carried out analytically.

3. A specific constitutive model

The developments discussed so far apply to any SMA model that can be specified in this context by a free energy density of the form (8) and a dissipation function of the form (12). The various features of the pseudoelastic behavior can be described at different levels of detail by specifying more or less sophisticated expressions of the two basic constitutive functions. Since the present work is aimed to highlight the applicability of the energetic approach to the study of the localization of the phase transformations in SMA, constitutive assumptions are kept to the maximum level of simplicity. In particular, from now on, the following assumptions will be enforced:

- constant elastic modulus $E'(\alpha) = 0$;
- constant interaction energy coefficient $\Omega'(\alpha) = 0$ subject to the constraint (9) with $\Omega > 0$;
- $M = \Omega\eta^2$ where $\eta := \sqrt{M/\Omega}$. As it will be seen it is useful to introduce the quantity η, since it has the dimension of a length and will be representative of the internal length of the material;
- driving force thresholds independent on the phase fraction

$$\Lambda'_F(\alpha) = 0, \qquad \Lambda'_R(\alpha) = 0 \tag{59}$$

Moreover, as already discussed, the behavior will be assumed to be isothermal with a uniform and constant temperature $T \geq A_f$. Summarizing, under the above simplifying assumptions, the two basic constitutive functions (8) and (12) take the following form:

$$\begin{aligned} \Phi(\varepsilon, \alpha, \gamma, T) =& \frac{E}{2}\left(\varepsilon - \mu\alpha\right)^2 + B_T\,\alpha + \Omega\,\alpha(1-\alpha) + \frac{\Omega\eta^2}{2}\gamma^2 + \Phi_0(T) \\ \Gamma(\alpha, \dot\alpha) =& \Lambda_{\mathrm{F}}\dot\alpha^+ + \Lambda_{\mathrm{R}}\dot\alpha^- \end{aligned} \tag{60}$$

where $B_T := B(T - T_e)$. Since $B > 0$ and $T > A_f > T_e$ it is $B_T > 0$. Taking into account (4) and (60) the constitutive equation for the stress is

$$\sigma = E(\varepsilon(x) - \mu\alpha(x)) \tag{61}$$

Evaluating it at the generic time t of a given process and using the corresponding boundary conditions, stress can be expressed, in terms of applied displacements, as

$$\sigma_t = E\left(\frac{U_t}{L} - \mu\,\langle\alpha_t\rangle\right) \quad \text{with} \quad \langle\alpha_t\rangle := \frac{1}{L}\int_0^L \alpha_t\,\mathrm{d}x \tag{62}$$

It turns out that the stress also depends on the the average value of the phase fraction over the bar. The driving forces (11) is

$$\Pi = E\,(\varepsilon - \mu\alpha)\,\mu + 2\Omega\alpha - B_T - \Omega + \Omega\eta^2\alpha'' \tag{63}$$

with E and Ω constant values. This expression clearly points out the nonlocal effect induced by the dependence of the free energy on the phase fraction gradient, namely the second spatial derivative of the phase fraction field acts as a driving force of the phase transformations. In particular an increase of α' acts like an increase of the stress.

3.1. Transformation criteria and kinetics

According to (56-58) Forward and Reverse Transformations can occur only in the regions $\overline{FwT}$ and $\overline{RvT}$ where the criteria $\Pi = \Lambda_{\mathrm{F}}$ and $\Pi = \Lambda_{\mathrm{R}}$ are respectively met. Taking into account (59), (61) and (63) the criteria can be written as:

$$\begin{aligned} \Omega\eta^2\,\alpha_t''(x) + 2\Omega\,\alpha_t(x) &= \mu(\sigma_{\mathrm{M}_S} - \sigma_t) \qquad x \in \overline{FwT} \\ \Omega\eta^2\,\alpha_t''(x) + 2\Omega\,\alpha_t(x) &= \mu(\sigma_{\mathrm{A}_F} - \sigma_t) \qquad x \in \overline{RvT} \end{aligned} \tag{64}$$

where, as it will be seen, the quantities

$$\sigma_{\mathrm{M}_S} := \frac{B_T + \Omega + \Lambda_{\mathrm{F}}}{\mu}, \qquad \sigma_{\mathrm{A}_F} := \frac{B_T + \Omega + \Lambda_{\mathrm{R}}}{\mu} \tag{65}$$

represent the values of stress at which the Forward and Reverse homogeneous transformations respectively starts and finishes.

If the phase fraction profile is homogeneous, each one of (64) reduces to an algebraic equation that can be solved for the unique value of the phase fraction that satisfies the criterion.

On the other hand, for non-homogeneous phase fraction profiles (64) give rise to stress-parameterized families of second-order differential equations in α_t. Since, by (62), the stress depends on the average value of the phase fraction, (64) turn out to be integro-differential equations of Fredholm type that can be solved by first integrating the differential equation with the stress as a parameter and then by computing its value by (62).

Moreover, (56-58) also require that the rate of change of phase fraction satisfy transformation kinetics of the type $\dot{\Pi} = \dot{\Lambda}_F$ and $\dot{\Pi} = \dot{\Lambda}_R$. Taking into account the specific expressions of the energetic quantities both kinetics take the same form

$$\Omega\eta^2\,\dot{\alpha}_t''(x) + 2\Omega\,\dot{\alpha}_t(x) = -\mu\dot{\sigma}_t \tag{66}$$

For non-homogeneous profiles this defines a family of differential equations in the field of rates $\dot{\alpha}_t$ parameterized by the stress-rate. But, the time derivative of a phase fraction field that satisfies (64) also satisfies (66), hence the possibility of evolution can be evaluated directly from the solutions of (64).

3.2. Stability analysis

For the specific model the second order stability (DS2) reads

$$\int_0^L E\,(\tilde{\varepsilon} - \mu\tilde{\alpha})^2 + \Omega\eta^2\,(\tilde{\gamma})^2 - (2\Omega)\,\tilde{\alpha}^2\,\mathrm{d}x \geq 0 \qquad \forall(\tilde{u},\tilde{\alpha}) \in \mathcal{S}_1(u_t,\alpha_t) \tag{67}$$

The left-hand side, that coincides with the second variation of the free energy, does not depend on the present state but only on the constitutive parameters. Therefore the stability analysis of any part of a process can be carried out at any instant within its domain of definition since it is not affected by the evolution.

The first two terms in (67) are non-negative while the third one is non-positive, hence the left-hand side has no lower bound in general. To enforce the non-negativity of (67) it is then convenient to introduce the Rayleigh ratio of the positive over the negative terms in (67), namely

$$\mathcal{R}(\tilde{u},\tilde{\alpha}) = \frac{\int_0^{\mathrm{L}} E\,(\tilde{u}' - \mu\,\tilde{\alpha})^2 \;\mathrm{d}x + \int_0^{\mathrm{L}} \Omega\,\eta^2 \tilde{\alpha}'^2 \;\mathrm{d}x}{\int_0^{\mathrm{L}} 2\Omega\,\tilde{\alpha}^2 \;\mathrm{d}x} \tag{68}$$

and compare it to the value 1. The second-order stability of the actual state can then be assessed as follows:

$$\min_{\mathcal{S}_1} \mathcal{R}(\tilde{u},\tilde{\alpha}) \begin{cases} > 1, & \Rightarrow \quad \text{the state } (u_t,\alpha_t) \text{ is stable} \\ < 1, & \Rightarrow \quad \text{the state } (u_t,\alpha_t) \text{ is unstable} \end{cases} \tag{69}$$

If the minimum is equal to 1, the second variation vanishes, nothing can be said about the character of the state and higher order directional stability conditions have to be investigated. The existence of the minimum (in the sense that it is reached by an admissible pair $(\tilde{u},\tilde{\alpha})$) over the convex subset $\mathcal{S}_1$ is guarantee by the strictly positiveness of $\mathcal{R}$, by virtue of the compactness of the injection of H^1 into L^2 and by the weak lower semi-continuity of a semi-norm, as in [38]. It is worth to remark that the minimum (69) has to be evaluated only with respect to those test directions that belongs to $\mathcal{S}_1$ where (DS1) is satisfied as an equality. It is then possible to consider the optimality with respect to $\tilde{u}$, namely $\mathcal{R}'(u,\tilde{\alpha})(v,0) = 0$, and to eliminate $\tilde{u}$ by minimizing $\mathcal{R}$ with respect to $\tilde{u}$ at given $\tilde{\alpha}$, specifically,

$$\mathcal{R}'(\tilde{\varepsilon},\tilde{\alpha})(v,0) = -\int_0^{\mathrm{L}} 2E\,(\tilde{\varepsilon} - \mu\,\tilde{\alpha})'\,v \;\mathrm{d}x + [2E\,(\tilde{\varepsilon} - \mu\,\tilde{\alpha})\,v]_0^L = 0$$

Taking into account the boundary conditions $v(0) = v(L) = 0$, it follows that $\tilde{\varepsilon} - \mu\,\tilde{\alpha} = k$ with k a constant. Recalling that $\tilde{\varepsilon} = \tilde{u}'$ and $\tilde{u}(0) = \tilde{u}(L) = 0$ it follows that the minimizing displacement test direction can be expressed in terms of $\tilde{\alpha}$ as

$$\tilde{u} = k\,x + \mu \int_0^x \tilde{\alpha} \;\mathrm{d}x, \qquad \text{with} \qquad k = -\frac{\mu}{L}\int_0^{\mathrm{L}} \tilde{\alpha} \;\mathrm{d}x \tag{70}$$

Substituting (70) into (68) one gets the reduced Rayleigh ratio depending only on the test direction for the phase fraction:

$$\mathcal{R}^*(\tilde{\alpha}) = \frac{\dfrac{E\mu^2}{L}\left(\int_0^{\mathrm{L}} \tilde{\alpha} \;\mathrm{d}x\right)^2 + \Omega\,\eta^2 \int_0^{\mathrm{L}} \tilde{\alpha}'^2 \;\mathrm{d}x}{2\Omega \int_0^{\mathrm{L}} \tilde{\alpha}^2 \;\mathrm{d}x} \tag{71}$$

such that

$$\min_{\mathcal{S}_1} \mathcal{R}(\tilde{u},\tilde{\alpha}) = \min_{\mathcal{S}_1^*} \mathcal{R}^*(\tilde{\alpha})$$

where $\mathcal{S}_1^* := \mathcal{S}_1 \div \mathcal{U}_0$. Even if the second variation does not depend on the state, different types of solutions may lead to a different stability analyses due to the fact that the set of directions $\mathcal{S}_1(u_t, \alpha_t)$ over which second-order stability needs to be tested may be different. Specific results follow in the next Sections.

4. Homogeneous processes

Spatially homogeneous states of the form

$$u_t(x) = xt, \qquad \alpha_t(x) =: \xi_t \tag{72}$$

correspond to the bar uniformly stretched with the same composition all over its length, ξ being the common value of the phase fraction. Due to the particular form assumed for the applied displacements (7), the uniform strain is numerically equal to the value of time, namely $\varepsilon_t(x) = t$. This choice helps to simplify notation and is irrelevant since the material response is rate-independent.

It is now shown that there is a unique process composed of homogeneous states of the form (72) which is a candidate solution for the loading-unloading displacement controlled tensile test.

The homogeneity of the phase fraction field implies that $\langle \alpha_t \rangle = \xi$ so that the stress is given by

$$\sigma_t = E\left(\frac{U_t}{L} - \mu\xi_t\right) \tag{73}$$

Initially the bar is fully austenitic and, taking into account (2), the driving force $\Pi(t) = E\mu t - B_T - \Omega$ is constant over the bar and increases with time. The initial driving force is negative since $B_T, \Omega > 0$, while irreversibility requires that $\Lambda_{\rm F} \geq 0$, hence $\Pi < \Lambda_{\rm F}$ so that, from (56), it follows that $\dot{\alpha}_t = 0$ hence $\xi_t = 0$. This corresponds to the elastic deformation of the purely austenitic bar that continues until the stress is equal to the value $\sigma_{{\rm M}_S}$ defined in (65) when the driving force attains the FwT threshold level $\Lambda_{\rm F}$ and the conditions for incipient Forward $A \to M$ Transformation over the whole bar, namely $\overline{FwT} = [0, L]$, are met. This happens at time

$$t_{\rm I} := \sigma_{{\rm M}_S}/E$$

when a simultaneous Forward Transformation of the whole bar may arise as a candidate solution. In fact, since $\alpha_t' = 0$ the criterion (64) reduces to an algebraic equation that can be solved for

$$\xi_t = \frac{\mu(\sigma_{{\rm M}_S} - \sigma)}{2\Omega} = \frac{E\mu}{E\mu^2 - 2\Omega}t - \frac{\mu\sigma_{{\rm M}_S}}{E\mu^2 - 2\Omega} \tag{74}$$

This solution can evolve in a FwT, according to (56), provided $E\mu^2 - 2\Omega > 0$ which holds by (9). Therefore at times $t > t_{\rm I}$ homogeneous FwT could take place, at constant rate, accompanied by the stress

$$\sigma_t = -\frac{2E\Omega}{E\mu^2 - 2\Omega}\left(t - \frac{E\mu^2}{2\Omega}t_{\rm I}\right) \tag{75}$$

This corresponds to stress softening, due to the positivity of Ω. Homogeneous Forward Transformation can proceed until the bar is fully transformed into pure martensite when the stress reaches the value

$$\sigma_{\mathrm{M}_F} := \frac{B_T - \Omega + \Lambda_{\mathrm{F}}}{\mu} = \sigma_{\mathrm{M}_S} - \frac{2\Omega}{\mu} \tag{76}$$

at time

$$t_{\mathrm{II}} := \sigma_{\mathrm{M}_F}/E + \mu$$

Further loading then involves elastic deformation of pure martensite since $\Pi > \Lambda_{\mathrm{R}}$. If unloading takes place after the completion of FwT, it induces a decrease of the driving force, hence elastic unloading of pure martensite until $\Pi = \Lambda_{\mathrm{R}}$ when the conditions for incipient Reverse $M \to A$ Transformation over the whole bar, namely $\overline{RvT} = [0, L]$, are met. Homogeneous RvT may then arise as candidate solution at constant rate with

$$\xi_t = \frac{\mu(\sigma_{\mathrm{A}_F} - \sigma_t)}{2\Omega} = \frac{E\mu}{E\mu^2 - 2\Omega}t - \frac{\mu\sigma_{\mathrm{A}_F}}{E\mu^2 - 2\Omega} \tag{77}$$

The complete reverse transformation takes place during the interval $[\bar{t}_I, \bar{t}_{II}]$ computed as above accompanied by a stress that increases from

$$\sigma_{\mathrm{A}_S} = \sigma_{\mathrm{A}_F} - \frac{2\Omega}{\mu} \tag{78}$$

to the value σ_{A_F} defined in (65). The slopes of the branches associated with FwT and RvT are equal and proportional to the ratio between interaction energy coefficient and the transformation strain. Moreover, hysteresis is determined by the difference between the thresholds for the two transformations

$$\sigma_{\mathrm{A}_S} - \sigma_{\mathrm{M}_F} = \frac{\Lambda_{\mathrm{R}} - \Lambda_{\mathrm{F}}}{\mu} \tag{79}$$

Since by (IR), $\Lambda_{\mathrm{R}} \leq 0 \leq \Lambda_{\mathrm{F}}$, irreversibility condition forces the stress line associated to RvT to be always below the FwT one.

Further unloading after RvT completion, at $t > \bar{t}_I$, involves elastic deformation of pure austenite since $\Pi < \Lambda_{\mathrm{F}}$. If unloading starts before the completion of FwT, namely at some phase fraction value $0 < \bar{\xi} < 1$, the situation is analogous to the previous one provided

$$\sigma_{\mathrm{A}_S}\left(\bar{\xi}\right) = \sigma_{\mathrm{A}_F} - \frac{2\Omega}{\mu}\bar{\xi} \tag{80}$$

4.1. Stability of the homogeneous responses

The homogeneous process just described is only a candidate solution as it satisfies first-order directional stability, energy balance and irreversibility. Hence to guarantee (DS), it is necessary to check second-order differential stability conditions with respect to the test directions for which first-order stability is satisfied as an equality. To this end, the situation is different for the various stages of the process.

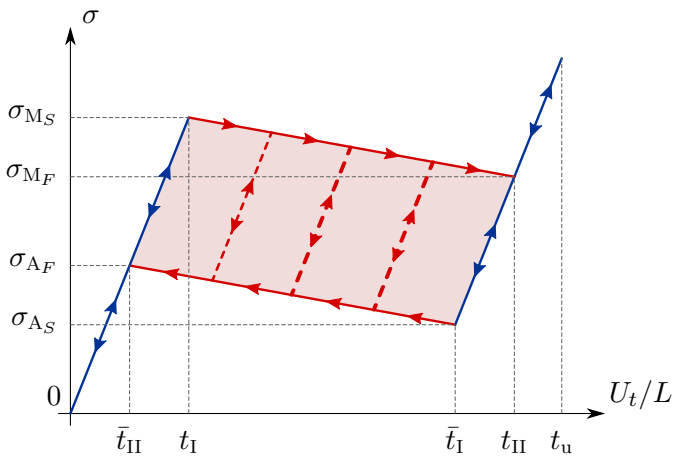

Figure 2: Global response for candidate solutions composed of homogeneous states.

During the elastic stage of pure austenite ($t < t_{\mathrm{I}}$) the first-order directional stability (DS1) is satisfied, over the whole bar, as an equality for all test directions of the form $(\tilde{u}, 0)$ due to (35), whereas it is satisfied as a strict inequality $\Pi < \Lambda_{\mathrm{F}}$ for all other directions. Therefore, second order stability have to be checked for continuations at fixed phase fraction. By evaluating (67) in this special case it follows that

$$\int_0^{\mathrm{L}} E\,\tilde{\varepsilon}^2\,\mathrm{d}x > 0 \qquad \forall \tilde{u} \in \mathcal{U}_0 \tag{81}$$

Since $E > 0$, the second-order directional stability is satisfied as a strict inequality and this is sufficient to guarantee full stability. By similar considerations it follows that all homogeneous elastic loading or unloading stages of the process are directionally stable and hence solutions of the evolution problem in the respective parts of the process.

During the Forward ($t_{\mathrm{I}} \le t < t_{\mathrm{II}}$) and Reverse ($\bar{t}_I < t \le \bar{t}_{II}$) Transformation stages the first-order stability is satisfied as an equality for test directions for which the phase transformation variation is respectively positive, $\mathcal{S}_1 = \mathcal{U}_0 \times \mathcal{V}^+_{\alpha_t}$ and negative $\mathcal{S}_1 = \mathcal{U}_0 \times \mathcal{V}^-_{\alpha_t}$. Then, limited to the Forward Transformation stage, the second-order stability (67) can be evaluated by minimizing the reduced Rayleigh ratio (71) that, after a change of variable $y := x/L$, can be expressed in the form:

$$\mathcal{R}^*(\tilde{\alpha}) = \frac{a\left(\int_0^1 \tilde{\alpha}\,\mathrm{d}y\right)^2 + b\int_0^1 (\tilde{\alpha}')^2\,\mathrm{d}y}{\int_0^1 \tilde{\alpha}^2\,\mathrm{d}y} \tag{82}$$

with

$$a := \frac{E\mu^2}{2\Omega} \qquad b := \frac{\eta^2}{2L^2}$$

As shown, for example in [38], it is possible to prove that

$$\min_{\mathcal{S}_1^*} \mathcal{R}^*(\tilde{\alpha}) = \min\left(a, \sqrt[3]{\pi^2 a^2 b}\right) \tag{83}$$

Taking into account the definitions of a and b and introducing a new notation for the normalized internal length

$$\ell_s := \frac{\pi a}{\sqrt{2}}\eta \tag{84}$$

the minimization (83) becomes

$$\min_{\mathcal{S}_{\mathrm{I}}^*} \mathcal{R}^*(\tilde{\alpha}) = \min\left(\frac{E\mu^2}{2\Omega}, \sqrt[3]{\frac{\ell_s^2}{L^2}}\right) \tag{85}$$

Due to the restrictions on the interaction energy coefficient (9), the first value in (85) is always greater than one, hence the stable or unstable character is determined by the second value. This latter depends, through ℓ_s defined by (84), on the material parameter η which governs the dependence of the free energy density on the phase fraction gradient as well as on the length L of the bar. It then follows that the stability of the homogeneous transformation is determined by the competition of ℓ_s and L so that:

$$\boxed{\begin{cases} L < \ell_s, & \text{the homogeneous transformation is stable} \\ L \geq \ell_s, & \text{the homogeneous transformation is unstable} \end{cases}} \tag{86}$$

If the bar is longer than ℓ_s the homogeneous transformation stage is unstable and therefore cannot be solutions of the evolution problem. Phase transformations have then necessarily to develop through spatially non-homogeneous phase fraction fields that will model localization phenomena. As the critical length ℓ_s does not depend upon the state variables, the stable or unstable character of the homogeneous response is immediately determined for the whole transformation stages regardless of time t. Figure 12 summarizes the stability results.

5. Non-homogeneous processes

As it will be discussed in Section 9, the internal length ℓ_s turns out to be rather small. Non-homogeneous responses have then to be searched, especially in the case $L > \ell_s$ where the homogeneous response is unstable. Nevertheless, the occurrence of non-homogeneous responses for $L \leq \ell_s$ can so far be expected which are here studied in detail.

The initial stage of the process ($t \leq t_{\mathrm{I}}$) corresponds, in any case, to elastic strain of the austenitic bar as in Section 4. Since it is $\Pi < \Lambda_{\mathrm{F}}$ over the whole bar, this gives a stable process until time t_{I} when the stress equals σ_{M_S} and there are conditions for incipient FwT over the whole bar. However, for $L > \ell_s$, the homogeneous transformation is unstable and non-homogeneous solutions will arise. This means that for $t > t_{\mathrm{I}}$ the FwT criterion has to be satisfied by phase fraction fields with $\alpha_t' \neq 0$. The first one of (64) then gives rise to a stress-parameterized linear second-order ODEs with constant coefficients formally analogous to the equation of motion of an undamped simple oscillator of "mass" $\Omega\eta^2$ and "stiffness" 2Ω subject to a constant "force" determined by the difference between the actual value of

the stress and the limit value σ_{M_s}. Since $2/\eta^2 > 0$ the general integral is oscillatory and can be written as

$$\alpha_t(x) = C_1 \cos\left(\frac{\pi}{\ell}x\right) + C_2 \sin\left(\frac{\pi}{\ell}x\right) + \frac{\mu(\sigma_{\mathrm{M}_S} - \sigma_t)}{2\Omega} \qquad x \in \overline{FwT} \tag{87}$$

with $\ell := \ell_s/a$ that defines another material internal length. This internal length strongly depends on the microstructure and is related to the phase transformation interface width, responsible of the sharp strain variation, arising bot in single-crystal SMA (kinematic compatibility reasons) and in poly-crystal SMA, [16, Fig. 15].

Eq. 87 corresponds to spatial oscillations of periodicity 2ℓ determined solely by the coefficient η that characterizes the dependence of the free energy density on the gradient of the phase fraction, whereas amplitude depends on the difference between the stress and the limit value σ_{M_S}. Comparing with (74) the constants-independent term in (87) turns out to be equal to the value of the phase fraction that would arise in an homogeneous transformation.

Forward Transformation must proceed with non-homogeneous phase fraction profiles for $L \geq \ell_s$ until the completion of the transformation at time t_{II}, but they could also occur for $\ell \leq L < \ell_s$. For $L < \ell$, non-homogeneous responses are not admissible, since any non-homogeneous phase transformation profile cannot satisfy (DS1), meaning that there is not enough space in the bar for the development of at least half oscillation, (88).

$$\boxed{\begin{cases} L < \ell, & \text{the non-homogeneous transformation is impossible} \\ L \geq \ell, & \text{the non-homogeneous transformation is stable} \end{cases}} \tag{88}$$

Unloading process then involve no transformation hence stable elastic strain, until the second criterion in (64) is attained over the set $\overline{RvT}$ at time $\bar{t}_I$. For each $t > \bar{t}_I$ phase fraction profile is then determined by a stress-parameterized ODE formally similar to the one for FwT, whose general integral is

$$\alpha_t(x) = C_3 \cos\left(\frac{\pi}{\ell}x\right) + C_4 \sin\left(\frac{\pi}{\ell}x\right) + \frac{\mu(\sigma_{\mathrm{A}_F} - \sigma_t)}{2\Omega} \qquad x \in \overline{RvT} \tag{89}$$

This differs from (87) only for the constant-independent term which is now equal to the value of the phase fraction that would arise in an homogeneous RvT (see (77)).

Since the stress depends on the average value of the phase fraction, the solutions depend on the geometry of the regions where transformation criteria are met. To this end several situations are possible, each one modeling different physical behaviors. While in real cases the nucleation of the localized transformation is triggered by the inhomogeneities of the various quantities that are induced by phenomena not taken into account in the model (like e.g. imperfections, stress concentrations and thermal effects), some basic cases will be discussed in detail.

5.1. Evolution of a full oscillation

There is a limit case in which a non-homogeneous candidate solution may develop with $\overline{FwT} = [0, L]$. This happens if $L = 2n\ell$ namely the length of the bar is exactly an even multiple of the internal length ℓ.

Concerning boundary conditions, consider the case in which (87) has a maximum in $x = 0$ and $\alpha(\ell) = 0$. This yields maxima at the two extremities and internal minima in pure austenite. The general integral (87) then yields

$$\alpha_t\,(x) = \bar{\alpha}_{\rm F}(\sigma_t)\cos^2\frac{\pi x}{2\ell} \qquad x \in [0, L] \tag{90}$$

This corresponds to a sinusoidal profile with the nucleation of a boundary localization of support ℓ at each end and $n-1$ inner localizations of support 2ℓ (Figure 3a). All localizations have a constant support and a common stress-dependent peak

$$\bar{\alpha}_{\rm F}(\sigma_t) := \frac{\mu\,(\sigma_{{\rm M}S} - \sigma_t)}{\Omega} \tag{91}$$

It is interesting to note that this is equal to twice the value of the fraction that would arise in an homogeneous transformation (see (74)). Substituting the average fraction, $\langle\alpha_t\rangle = \bar{\alpha}_{\rm F}(\sigma)/2$, into (62) it follows that the localizations grow accompanied by a stress softening governed by the same law (75) of the homogeneous solutions. The explicit form of the phase fraction profile during the first part of the FwT then becomes

$$\alpha_t\,(x) = \frac{2E\mu\,(t - t_{\rm I})}{E\mu^2 - 2\Omega}\cos^2\frac{\pi\,(\ell - x)}{2\ell} \quad x \in [0, L] \tag{92}$$

The growth of the localizations proceed until time $t_{\rm III} = t_{\rm I} + (E\mu^2 - 2\Omega)/(2E\mu)$ when the stress is equal to

$$\sigma_{{\rm M}P} = \sigma_{{\rm M}S} - \frac{\Omega}{\mu} \tag{93}$$

At this moment the FwT transformation is complete at the peaks of the localizations. The stress level (93) at which growth is complete turns out to be equal to the mean of the values σ_{Ms} and σ_{Mf} at which the homogeneous transformation starts and finishes. Computation of the stress shows that the stress evolution is the same as for the homogeneous transformation.

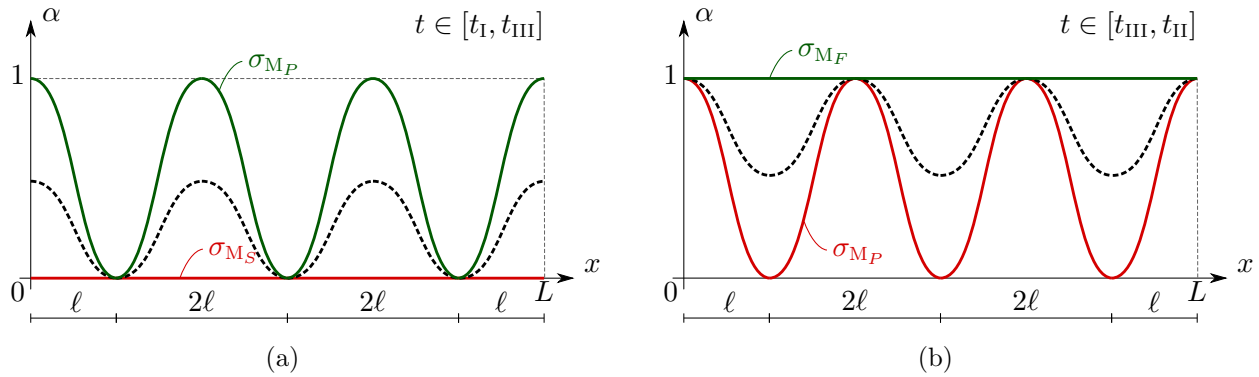

Figure 3: Evolution during FwT of non-homogeneous phase fraction profiles with full oscillation in the case of $L = 6\ell$: growth (left) and coalescence (right).

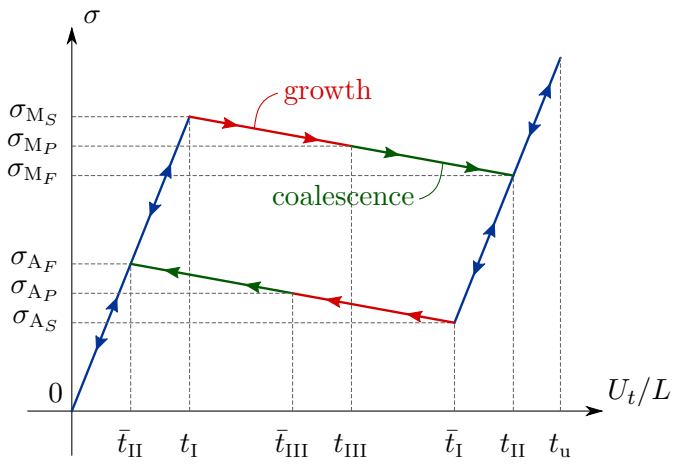

Figure 4: Global response associated with non-homogeneous phase fraction profiles with full oscillation. The behavior is analogous to the one of homogeneous transformation but with completely different evolution of the phase fraction profiles.

A further reduction of the stress with the profile (92) would give points with $\alpha > 1$ hence a different profile has to evolve. Imposing new boundary conditions $\alpha_t(0) = 1$ and $\bar{x} = 0$ a different solution emerges from (87), so that for $t > t_{III}$ the phase fraction profile is given by

$$\alpha_t(x) = 1 - 2\left(1 - \frac{E\mu\,(t - t_I)}{E\mu^2 - 2\Omega}\right)\cos^2\frac{\pi\,(x - \ell)}{2\ell}$$

As shown in Figure 3b this corresponds to a dual sinusoid with n "valleys" growing toward the coalescence with the already transformed regions. This second stage is accompanied again by stress softening analogous to the one of the homogeneous solution. The transformation is complete when the whole bar is fully converted to martensite and this happens at time t_{II} when the stress is equal to σ_{M_F}.

Loading and unloading after the completion of the FwT leads to elastic strain of the pure martensite until the reverse transformation takes place with $\overline{RvT} = [0, L]$ giving rise to nucleation, growth and coalescence of sinusoidal profiles that mirror those formed during FwT but with stress levels

$$\sigma_{A_S}, \quad \sigma_{A_P} := \frac{\sigma_{A_S} + \sigma_{A_F}}{2}, \quad \sigma_{A_F} \tag{94}$$

corresponding respectively to σ_{M_S}, σ_{M_P} and σ_{M_F} of Figure 3b.

This describes another candidate solution derived on the basis of first-order stability. The investigation of its full stability is analogous to the one already discussed for the homogeneous solution and shows that such non-homogeneous transformation with fully oscillating profiles is again unstable and therefore different types of non-homogeneous solutions with disjointed localizations have to be searched. The global response associated to non-homogeneous phase fraction profiles with full oscillation is depicted qualitatively in Figure 4.

5.2. Basic types of localizations

The case discussed in the preceding Section is very special since it could, eventually, take place only in the unlikely situation of a bar of length equal to an exact even multiple of ℓ. In practice this would never be the case and therefore the full oscillation will not develop due to the impossibility to fulfill boundary conditions (in addition to the fact that it would be unstable anyway). Spatially non-homogeneous responses will, in general, arise with the transformation criteria attained as an equality over strict subsets of the whole bar. To this end there are various possibilities. First of all, it may happen that the potentially transforming sets can be expressed as the union of connected components $\overline{FwT}_i$ and $\overline{RvT}_i$ where the criteria (64) hold.

$$\overline{FwT} = \bigcup_i \overline{FwT}_i \subset [0, L], \qquad \overline{RvT} = \bigcup_i \overline{RvT}_i \subset [0, L] \tag{95}$$

The nucleation of several disjoint regions corresponds to the case of multiple localizations. However, irrespective of the number of localizations, within each one of them the phase fraction profiles are necessarily determined by (64). The general integrals (87) and (89) have then to be computed explicitly in each component by imposing suitable boundary conditions that ensure consistency with the fact that in the rest of the bar the first-order stability is satisfied as a strict inequality and transformations cannot occur. This means that a general non-homogeneous phase fraction profile is obtained as the union of three types of regions: boundary localizations, inner localizations, non-transforming zones.

In Appendix A closed form expressions of the phase fraction profile are given for the six cases that can be considered as the basic building blocks for more general situations.

5.2.1. Boundary localizations

As shown in Figure 5, the minimal localizations that may arise in FwT correspond to half oscillations over a support of length ℓ near the boundary.

Localizations of type (a) and (c), described in Figure 5a and Figure 5c, typically model the nucleation from pure austenite of a martensite region near the ends of the bar. According to (A.2) and (A.5) such profiles have a stress-dependent peak equal to $\bar{\alpha}_{\mathrm{F}}(\sigma)$ defined in (91). At $\sigma = \sigma_{\mathrm{M}_S}$ the profiles degenerate into pure austenite, while the maximum grows under decreasing stress until $\sigma = \sigma_{\mathrm{M}_P}$ (see (93)) when the peak is completely transformed into martensite.

Localizations of type (b) and (d) (Figure 5b, Figure 5d), typically model the coalescence of a region near the ends of the bar with the rest of the bar already transformed to pure martensite. According to (A.3) and (A.6) such profiles have a stress-dependent minimum given by (A.4). At $\sigma = \sigma_{\mathrm{M}_P}$ the profile consists of a partially transformed region with the right end still in pure austenite, the minimum value grows under decreasing stress until $\sigma = \sigma_{\mathrm{M}_F}$ when it degenerates into pure martensite.

This discussion applies to profiles that may arise in FwT. A similar discussion can be carried out to characterize the profiles that may arise in RvT. Analogous shapes can be obtained but at different stress levels, in particular the roles of $\sigma_{\mathrm{M}_S}, \sigma_{\mathrm{M}_P}, \sigma_{\mathrm{M}_F}$ are replaced by the corresponding values $\sigma_{\mathrm{A}_S}, \sigma_{\mathrm{A}_P}, \sigma_{\mathrm{A}_F}$.

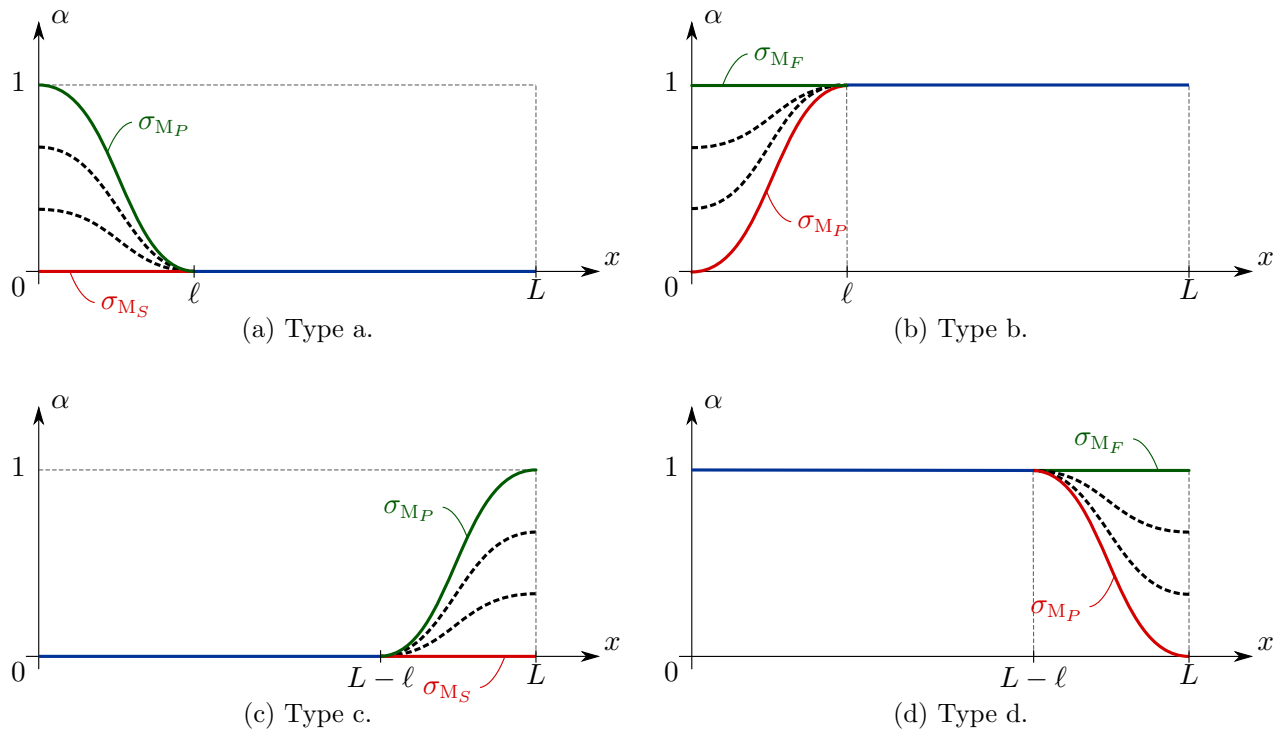

Figure 5: The four basic types of boundary localizations that may occur in FwT. The profiles that may occur in RvT are analogous provided the stress levels are varied accordingly.

5.2.2. Inner localizations

Localizations may also arise in the interior of the bar. As shown in Figure 6, the minimal inner localization corresponds to a complete oscillation over a support of length 2ℓ centered around some internal point x_i.

Localizations of the type (e) (Figure 6a) typically model the nucleation in a region of a martensite in the interior of the bar. According to (A.7) this has a stress-dependent maximum equal to $\bar{\alpha}_{\mathrm{F}}(\sigma)$ as for localizations of type (a) and (c). Similarly at $\sigma = \sigma_{M_S}$ it degenerate into pure austenite, while the maximum grows under decreasing stress until $\sigma = \sigma_{M_P}$ when the peak is completely transformed into martensite.

Localizations of type (f) (Figure 6b), typically model the coalescence of an internal region with the rest of the bar already transformed to pure martensite. According to (A.8) this has a stress-dependent minimum equal to the one of types (b) and (d) so that at $\sigma = \sigma_{M_F}$ it degenerates into pure martensite.

Concerning RvT, as discussed in previous Section, analogous profiles may arise at the suitable stress levels.

6. Evolution of a single boundary localization

Experimental evidence shows that under isothermal conditions a single localization tends to form. Multiple localizations are, on the other hand, typical of the non-isothermal setting as a consequence of the fact that nucleation stresses are temperature-dependent and the temperature tends to change due to the latent heat associated with the phase transformations.

In the following, the simplest case where a single boundary localization nucleates at the left end will be discussed. This situation may be considered as one of the most common as it can usually be triggered by stress concentrations at the grip.

6.1. Nucleation and growth

A left boundary localization can nucleate at time t_{I} if $\overline{FwT} = [0, \ell]$. As discussed in the previous Section this gives rise to an half-sinusoid of type (a) (Figure 5) with a stress-dependent peak that grows under decreasing stress. During growth the support of the localization remains constantly equal to ℓ hence it is determined solely by the parameter η in the free energy density.

The growth phase ends when stress is equal to σ_{M_P} and the left end is completely transformed into martensite. The stress drop needed for the complete growth of the localization is equal to the ratio between the transformation strain and the interaction energy coefficient because of

$$\sigma_{\mathrm{M}_S} - \sigma_{\mathrm{M}_P} = \frac{\Omega}{\mu} \tag{96}$$

To complete the determination of the candidate solution the actual value of the stress has to be computed for times $t > t_{\mathrm{I}}$. The average value of the phase fraction profile (A.2) is

$$\langle \alpha_t \rangle = \frac{\bar{\alpha}_{\mathrm{F}}(\sigma)}{2} \frac{\ell}{L} \tag{97}$$

which inserted into (62) yields to the stress

$$\sigma_t = -\frac{2\Omega E}{E\mu^2\ell - 2\Omega L}\left(Lt - \frac{E\mu^2}{2\Omega}\ell t_{\mathrm{I}}\right) = \frac{L}{\ell_s - L}\left(\frac{\ell_s}{L}\sigma_{\mathrm{M}_S} - Et\right) \tag{98}$$

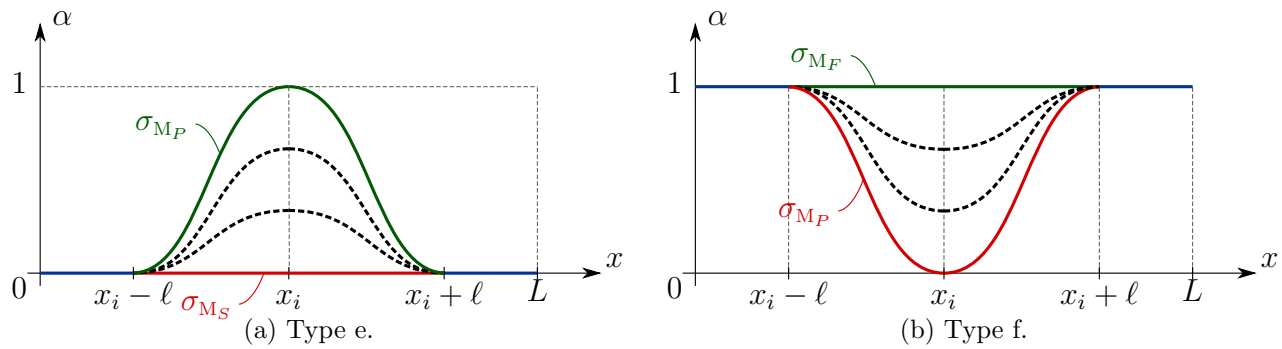

(a) Type e. (b) Type f.

Figure 6: The two basic types of inner localizations that may occur in FwT. The profiles that may occur in RvT are analogous provided the stress levels are varied accordingly.

It turns out that the denominator of the first factor above can be either positive or negative depending on the length of the bar. Suppose for the moment that $L \leq \ell_s$, namely that the bar is so short that the denominator is positive. This means that attention is restricted to bars of length $\ell \leq L < \ell_s$, which makes sense since, due to (9), it turns out that $\ell < \ell_s$. It is worth nothing that for such bar lengths the homogeneous solution is also stable such that both homogeneous and non-homogeneous responses can be admissible. This possibility has already been noticed and commented in the context of damage mechanics, [38].

Substituting (98) into (A.2) the explicit form of the phase fraction profile as a function of time is

$$\alpha_t(x) = \begin{cases} \left(\dfrac{E\mu(t-t_{\rm I})}{\Omega}\dfrac{L}{\ell_s - L}\right)\cos^2\left(\dfrac{\pi}{2\ell}x\right) & x \in [0,\ell] \\ 0 & x \in [\ell, L] \end{cases} \tag{99}$$

At time $t_{\rm I}$ this reduces to homogeneous austenite, whereas at later times the nucleation grows accompanied by a stress decrease determined by (98).

The expressions (98) and (99) also show that the slowest possible softening and transformation rates are obtained for the shortest bar $L = \ell$ (Figure 7). On the other hand transformation rates are faster and faster for longer bars. In the limit case of $L = \ell_s$, infinite rates are obtained and this can be interpreted as the occurrence of a snap-back characterized by a sudden localized transformation accompanied by an instantaneous stress drop from $\sigma_{{\rm M}_S}$ to $\sigma_{{\rm M}_P}$. The same phenomenon has necessarily to occur also for bars longer than ℓ_s in order not to contradict causality of time evolution. This effect is shown in the experimental test of Figure 15. The growth of the boundary nucleation is then completed at time

$$t_{\rm III} = \begin{cases} t_{\rm I} + \dfrac{\Omega}{E\mu}\left(\dfrac{\ell_s}{L} - 1\right) & \text{if } \ell \leq L < \ell_s \\ t_{\rm I} & \text{if } L \geq \ell_s \end{cases} \tag{100}$$

Therefore if the length of the bar is bounded by ℓ_s and ℓ then $t_{\rm III} > t_{\rm I}$ and the effects of the localization growth are observable as a non-sharp peak in the displacement controlled traction test (Figure 7). The quantity ℓ_s can then be interpreted not only as a stability internal length but also as a snap-back length, providing the occurrence of a single boundary localization. In case of multiple localizations, discussed in the next section, the stability internal length ℓ_s will differ from the snap-back length which thus will be denoted L_s ($\geq \ell_s$).

6.2. Front propagation

At time $t_{\rm III}$ the bar is in pure martensite at the left end and the bar is partitioned in the zone $\overline{FwT} = [0, \ell]$ where the transformation criterion $\Pi = \Lambda_{\rm F}$ is satisfied as an equality and the remaining zone where $\Pi < \Lambda_{\rm F}$ in pure austenite. A further decrease of the stress would produce points with $\alpha > 1$ which is meaningless. On the other hand, a stress increase would produce a decrease of the phase fraction which is inconsistent with the occurrence of FwT. However, the transformation can proceed at *constant stress* $\sigma = \sigma_{{\rm M}_P}$ provided the average phase fraction increases

$$\langle \alpha_t \rangle = \frac{1}{\mu}t - \frac{\sigma_{{\rm M}_P}}{E\mu}$$

Since, as just discussed, this cannot be produced by a growth of the localization in $[0, \ell]$, the increase of the applied displacements can induce a front propagation described by

$$\overline{FwT}(t) = [l(t), l(t) + \ell]$$

where $l(t)$ indicates the length of the boundary region converted to pure martensite (Figure 8). This corresponds to to a phase fraction profile

$$\alpha_t(x) = \begin{cases} 1 & x \in [0, l(t)] \\ \cos^2 \dfrac{\pi(x - l(t))}{2\ell} & x \in [l(t), l(t) + \ell] \\ 0 & x \in [l(t) + \ell, L] \end{cases}$$

The length $l(t)$ can be computed by substituting the value of the average phase fraction into the expression of the stress

$$l(t) = \frac{L}{\mu}(t - t_{\mathrm{I}}) + \frac{\Omega}{E\mu^2}(L - \ell_s) \tag{101}$$

If $L < \ell_s$ it follows that $l(t_{\mathrm{III}}) = 0$ hence propagation proceeds smoothly, whereas if $L \geq \ell_s$

$$l(t_{\mathrm{III}}) = \frac{\Omega}{E\mu^2}(L - \ell_s) \tag{102}$$

this gives a jump in the length of the transformed zone. Propagation is possible until the rightest point of the front reaches the right-end where there is no space to enlarge the fully transformed zone without modifying the localization shape (Figure 8). This happens at time t_{IV} such that $\ell + l(t_{\mathrm{IV}}) = L$ that is

$$t_{\mathrm{IV}} = t_{\mathrm{I}} + \left(\mu - \frac{\Omega}{E\mu}\left(\frac{L + \ell_s}{L}\right)\right)$$

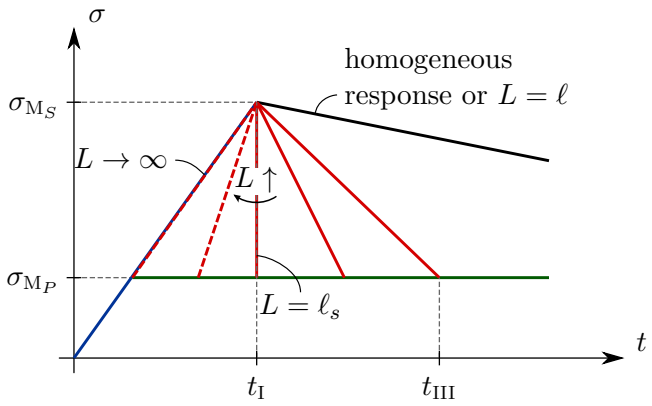

Figure 7: Detail of the response at the onset of the phase transformation and following localization process. The snap-back response occurrence is highlighted as well the limit behaviors depending on the bar length. The effect of an increasing bar length is the same of a decreasing internal length η.

It turns out that time needed to complete the propagation increases with the length of the bar. The earliest possible occurrence for t_{IV} arises in the case of a bar with $L = \ell$. For longer bars the propagation completion takes longer time and, in particular, it is $t_{\mathrm{IV}} = t_{\mathrm{II}}$ for $L = \ell_s$ (Figure 9).

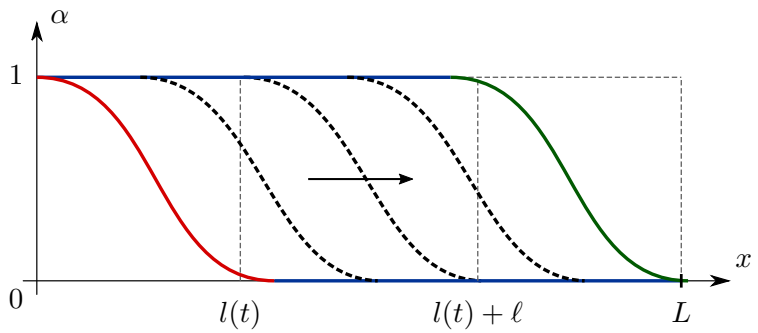

Figure 8: Schematic representation of the propagation of the left boundary localization.

6.3. Coalescence and transformation completion

At time t_{IV} propagation at constant stress is no longer possible since there is no space to further enlarge the region of fully transformed points. At this time a further reduction of stress is possible via the modification of the phase fraction profile which is now possible due to the possibility to impose different boundary conditions on (87). This gives rise to a right boundary localization of type (d). As already discussed the minimum increases for decreasing stress which evolves according to

$$\sigma_t = E\frac{\ell_s}{L-\ell_s}\left(\frac{L}{\ell_s}t - t_{\mathrm{I}}\right) + \frac{2\Omega\ell_s - E\mu^2 L}{\mu\,(L-\ell_s)}$$

At time $t = t_{\mathrm{IV}}$ this correctly reduces to σ_{M_P}. Substituting it into (A.6) the explicit expression of the phase fraction profile is obtained

$$\alpha_t(x) = \begin{cases} 1, & \text{if } x \in [0, L-\ell) \\ 1 - \left(\dfrac{L}{L-\ell_s}\left(\dfrac{2\Omega - E\mu^2}{\Omega} + \dfrac{E\mu\,(t-t_{\mathrm{I}})}{\Omega}\right)\right)\cos^2\dfrac{\pi\,(L-x)}{2\ell}, & \text{if } x \in [L-\ell, L] \end{cases} \tag{103}$$

This profile has a minimum equal to

$$\alpha_{\min} = 1 - \left(\frac{L}{L-\ell_s}\left(\frac{2\Omega - E\mu^2}{\Omega} + \frac{E\mu\,(t-t_{\mathrm{I}})}{\Omega}\right)\right) \tag{104}$$

that increases with time. The transformation is completed when the minimum is equal to 1 and this happens at the same time t_{II} at which the homogeneous FwT completes and the stress is equal to σ_{M_F}. Non-homogeneous FwT is then completed at the same instant and at

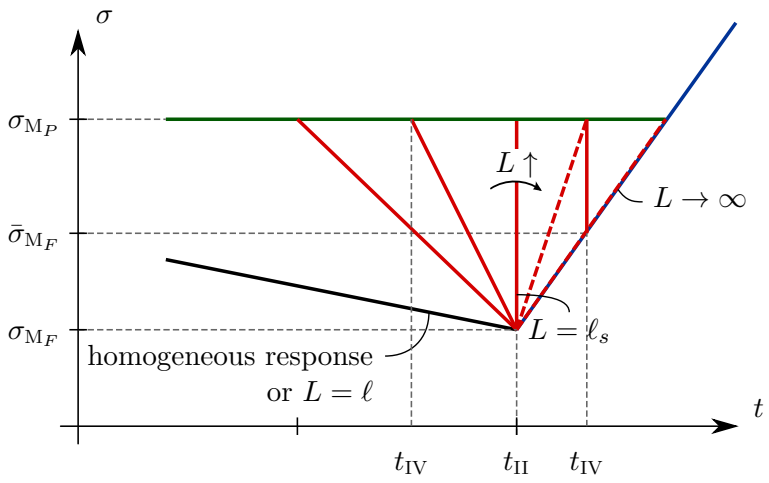

Figure 9: Detail of the response at the end of the phase transformation and following coalescence process. The snap-back response occurrence is highlighted as well the limit behaviors depending on the bar length. The effect of an increasing bar length is the same of a decreasing internal length η.

the same stress level at which the homogeneous transformation would complete, irrespective of the length of the bar.

The formulas for σ_t and for the instant t_{II} at which propagation is complete show that there are again two possible situations (Figure 9).

If $\ell \leq L < \ell_s$ it turns out that $t_{\mathrm{IV}} < t_{\mathrm{II}}$ so that the transformation completion occurs with stress decreasing linearly from σ_{M_P} to σ_{M_F} in the time interval $[t_{\mathrm{IV}}, t_{\mathrm{II}}]$. The stress rate is faster for longer bars and in the limit case of $L = \ell_s$ an infinite the stress rate is obtained. Propagation completion then takes place at the same time at which coalescence completes,

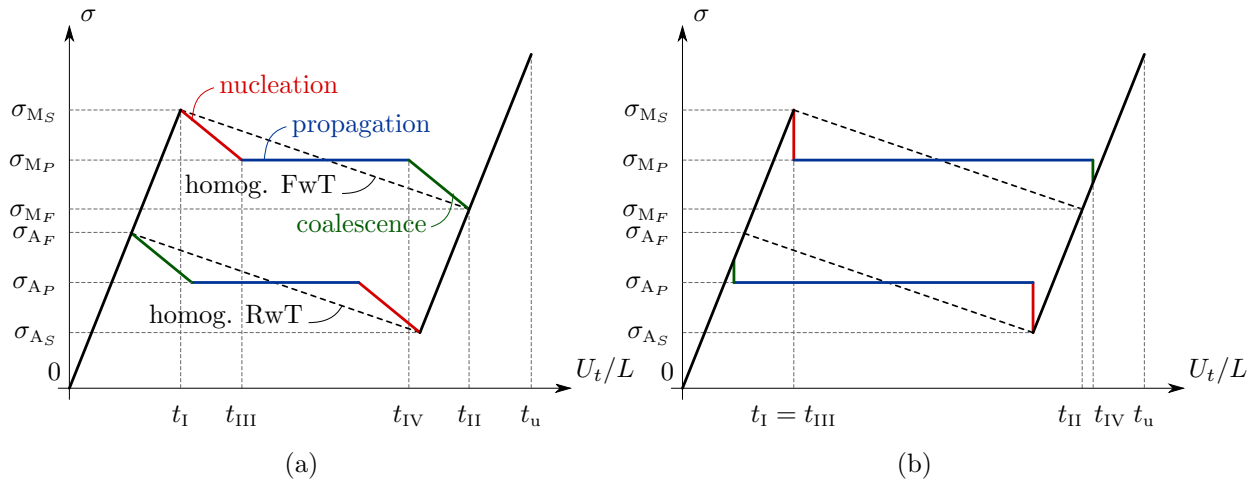

Figure 10: Global stress-displacement response with a single boundary localization and the occurrence of snap-back phenomena depending on the length of the bar: $\ell \leq L < \ell_s$ (left) and $L \geq \ell_s$ (right)

namely $t_{\rm IV} = t_V = t_{\rm II}$ This may be interpreted again as the occurrence of a snap-back after which the bar suddenly becomes fully martensitic and the localization disappears with an instantaneous stress drop from $\sigma_{{\rm M}_P}$ to $\sigma_{{\rm M}_F}$ (Figure 9).

For longer bars $L \geq \ell_s$ it would be $t_{\rm IV} > t_{\rm II}$ but this again would violate the causality of time evolution hence this can be interpreted as the occurrence of a snap-back, at time $t_{\rm IV}$ with instantaneous completion of the transformation. In this case, as soon as the transformation is completed the first-order stability is immediately satisfied as $\Pi > \Lambda_{\rm R}$ and the global response curve drops to the curve corresponding to elastic strain of pure martensite at stress level

$$\bar{\sigma}_{{\rm M}_F} = E(t_{\rm IV} + \mu)$$

generally greater than $\sigma_{{\rm M}_F}$ (Figure 9)). This means that the stress drop associated with the coalescence of the last untransformed region is generally smaller than the one associated with the nucleation. Specifically it is smaller the longer is the bar and it vanishes in the limit of $L \to \infty$ (Figure 9). For this reason it is much more difficult to capture in experiments such stress peak, although a trace of it can be found in [51].

6.4. Reverse transformation

If applied displacements are further increased after completion of the FwT, there is again stable elastic loading of the bar fully of pure austenite. If unloading occurs thereafter a discussion analogous the the previous one can be carried out, provided the stress values are modified accordingly. Figure 10 explains the situation by showing the global response.

7. General non-homogeneous responses

After the discussion of the basic case of a single boundary localization, more complex cases, where multiple localizations nucleates and evolve, can be treated as well.

7.1. Nucleation

Non-homogeneous phase fraction profiles may nucleate at $\sigma = \sigma_{{\rm M}_S}$ in FwT or at $\sigma = \sigma_{{\rm A}_S}$ in RvT when the bar is partitioned as the union of disjointed regions where one of the criteria (64) is met and the rest of the bar where first-order stability is satisfied as a strict inequality and transformations do not occur, denoted NoT as in (31).

Multiple localizations nucleate when the sets (95) are, in turn, the union of two or more intervals where the solutions (87) and (89) have to be evaluated with suitable boundary conditions. Each one of such intervals can be either a boundary localization with support equal to an odd multiple of ℓ or an inner localization with support equal to an even multiple of ℓ. Hence, a general solution can be composed by n full localizations taking place over a support of 2ℓ and m half-localizations supported over a length ℓ (provided, of course, $(2n + m)\ell \leq L$ and $0 \leq m \leq 2$).

7.2. Growth

From the results shown in Appendix A it follows that, during growth, all localizations have fixed support and extrema completely determined by the value of the stress. Therefore multiple localizations necessarily grow simultaneously with a common maximum or minimum.

In the case of FwT this occur in the stress range $\sigma_{\mathrm{M}_P} < \sigma < \sigma_{\mathrm{M}_S}$ where localizations of types (a), (c), (e) can occur all of them matched with pure austenite without points in pure martensite. The average phase fraction is then given by

$$\langle \alpha_t \rangle = \left(\frac{\mu \left(\sigma_{\mathrm{M}_S} - \sigma \right)}{\Omega} \right) \left(\frac{2n+m}{2} \right) \frac{\ell}{L}$$

and stress evolves according to

$$\sigma_t = \frac{L_s \, \sigma_{\mathrm{M}_S} - ELt}{L_s - L} \tag{105}$$

where

$$L_s := (2n+m)\ell_s \tag{106}$$

The growth may be either gradual of sudden depending on the possible occurrence of a snap-back. Eq. (105) shows that the presence of multiple localizations influences the snap-back length L_s which is proportional to the total length of the region $\overline{FwT}$ and the stability internal length, (106). Therefore the more localizations occur the more likely is to observe a non-sharp nucleation peak,

$$\boxed{\begin{cases} L < L_s, & \text{the non-homogeneous transformation has no snap-backs} \\ L \geq L_s, & \text{the non-homogeneous transformation has snap-backs} \end{cases}} \tag{107}$$

7.3. Propagation and coalescence

The growth phase proceeds until the points where extreme values occur are converted into a pure phase. In FwT this can only occur at the stress level σ_{M_P} when all localizations have a common peak in pure martensite. At this time growth is no longer possible as it would produce non admissible values of the phase fraction. If the non-transforming set NoT is not empty, propagation at constant stress takes place by enlarging the region where transformation is complete until the region NoT vanishes. At this stage boundary localizations may translate while inner localizations may either translate or split into pairs of moving half localizations (Figure 11). The length $l(t)$ of the completed transformation region in (101) can still be computed by the same formula provided the suitable value of L_s is used. In presence of multiple localizations it is correlated with the distance between the transformation fronts. More precisely, in the case of a single inner localization, it is indeed equal to the distance between the two propagating fronts. In presence of multiple boundary and inner localizations $l(t)$ is equal to the sum of the lengths $l_i(t)$ of all intervals where transformation is completed, so that $L - l(t)$ is the sum of the distances between all the fronts (Figure 11). The model then predicts that the sum of all distances between the fronts increases at constant rate and this is consistent with the experimental observations [42].

When the region NoT is empty, there is no room for front propagation with phase fraction profile of the same shape and the coalescence of the regions, non completely transformed, occur. This generally entails a reduction of the stress in the interval $\sigma_{\mathrm{M}_F} < \sigma < \sigma_{\mathrm{M}_P}$ when localizations of type (b), (d), (f) can take place with or without snap-back depending on the length of the bar.

8. The stability of the non-homogeneous responses

The study of the stability of non-homogeneous solutions has proved to be a prohibitive task in gradient-damage models [38] since the second-order stability conditions strongly depend on the localization itself. Similar considerations apply also to the SMA model in [24]. On the contrary, here the second variation of the free energy does not depend directly upon the state variables and the stability of non-homogeneous candidate solutions can be carried out in a straightforward way.

The full stability of elastic loading and unloading has been already proven in Section 4.1. It remains to check the non-homogeneous transformation stages.

Second-order stability has to be evaluated over the set $\mathcal{S}_1$, defined in (26), of test directions with respect to which first-order stability is satisfied as an equality. In this case, this means that the only relevant test directions $\tilde{\alpha}$ are those that vanish outside the regions $\overline{FwT}$ or $\overline{RvT}$ while are respectively non-negative and non-positive inside, namely

$$\mathcal{S}_1(u_t, \alpha_t) = \{(\tilde{u}, \tilde{\alpha}) \in \mathcal{U}_0 \times \mathcal{V}_\alpha \mid \begin{cases} \tilde{\alpha}(x) \geq 0, & \text{if } x \in \overline{FwT} \\ \tilde{\alpha}(x) \leq 0, & \text{if } x \in \overline{RvT} \\ \tilde{\alpha}(x) = 0, & \text{otherwise} \end{cases} \} \tag{108}$$

But, according to (95) the sets where transformation criteria are met are, in general, the union of several connected components and moreover, as discussed in Section 7, each component corresponds either to a full localization of support 2ℓ or to an half-localization of support ℓ.

Attention can then be focused on a general non-homogeneous response composed by n full localizations supported over the intervals F_i and m half-localizations supported over the

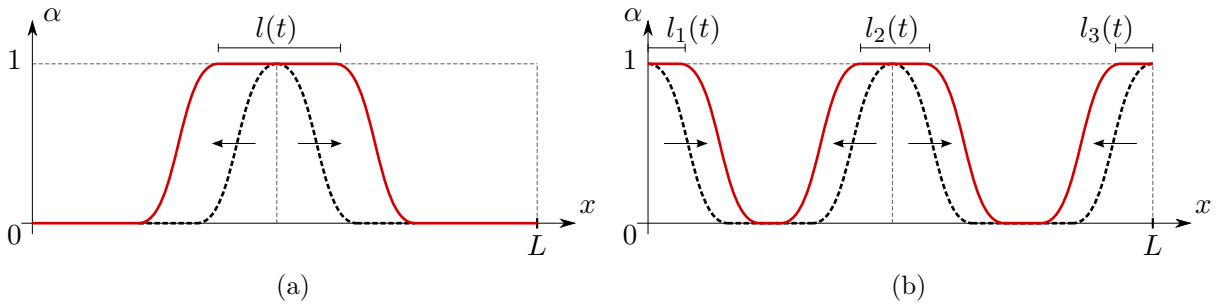

Figure 11: Propagation of an inner localization (left) and of one inner and two boundary localizations (right) to illustrate the meaning of the length $l(t)$.

intervals H_j (provided, of course $(2n+m)\ell \le L$) all disjointed. This response can be assumed to arise either in FwT or in RvT, the difference being the type of profiles. The Rayleigh ratio is then given by

$$\mathcal{R}(\tilde{u},\tilde{\alpha}) = \frac{\displaystyle\sum_{i=1}^{n}\Big(\int_{F_i}\big(E\,(\tilde{u}'-\mu\,\tilde{\alpha})^2+\Omega\,\eta^2\tilde{\alpha}'\big)^2\,\mathrm{d}x\Big)+\sum_{j=1}^{m}\Big(\int_{H_j}\big(E\,(\tilde{u}'-\mu\tilde{\alpha}^2)+\Omega\eta^2\tilde{\alpha}'^2\big)\,\mathrm{d}x\Big)}{\displaystyle\sum_{i=1}^{n}\Big(2\Omega\int_{F_i}\tilde{\alpha}^2\,\mathrm{d}x\Big)+\sum_{j=1}^{m}\big(2\Omega\int_{H^j}\tilde{\alpha}^2\,\mathrm{d}x\big)}$$

Since the minimum of the Rayleigh ratio has to be compared with the value 1 and each addend in the sums is a positive term, the stability of the non-homogeneous state reduces to

$$\min_{\mathcal{S}_1}\left((\mathcal{R}_F(\tilde{u},\tilde{\alpha}),\mathcal{R}_H(\tilde{u},\tilde{\alpha})\right)\begin{cases}>1, & \Rightarrow \quad \text{the state } (u,\alpha) \text{ is stable}\\ <1, & \Rightarrow \quad \text{the state } (u,\alpha) \text{ is unstable}\end{cases} \tag{109}$$

where

$$\mathcal{R}_F(\tilde{u},\tilde{\alpha})=\frac{\int_0^{2\ell}\big(E\,(\tilde{u}'-\mu\,\tilde{\alpha})^2+\Omega\,\eta^2\tilde{\alpha}'^2\big)\,\mathrm{d}x}{2\Omega\int_0^{2\ell}\tilde{\alpha}^2\,\mathrm{d}x},\quad \mathcal{R}_H(\tilde{u},\tilde{\alpha})=\frac{\int_0^{\ell}\big(E\,(\tilde{u}'-\mu\,\tilde{\alpha})^2+\Omega\,\eta^2\tilde{\alpha}'^2\big)\,\mathrm{d}x}{2\Omega\int_0^{\ell}\tilde{\alpha}^2\,\mathrm{d}x}. \tag{110}$$

The choice of the limits of integration in (110) is immaterial since the Rayleigh ratio does not depend upon the actual state, so that they simply have to be such that the integration domain correspond to a full, F_i, or half, H_j, localization.

Eliminating the field $\tilde{u}$ as in Section 3.2 and performing a change of integration variable as in Section 4.1, the ratios (110) can be reduced to ratios $\hat{\mathcal{R}}_F$ and $\hat{\mathcal{R}}_H$ of the form (82) with

$$a=\frac{\mu^2 E}{2\Omega},\quad \text{for both } \hat{\mathcal{R}}_F \text{ and } \hat{\mathcal{R}}_H,\qquad \text{and}\qquad b=\begin{cases}\eta^2/8\ell^2=1/4\pi^2, & \text{for } \hat{\mathcal{R}}_F\\ \eta^2/2\ell^2=1/\pi^2, & \text{for } \hat{\mathcal{R}}_H\end{cases} \tag{111}$$

Invoking again the result (83) it follows that

$$\min_{\mathcal{S}_1^*}\hat{\mathcal{R}}_F=\min\Big(a,\sqrt[3]{4\pi^2a^2b}\Big)=\min\Big(a,\sqrt[3]{\ell_s^2/\ell^2}\Big) \tag{112}$$

while

$$\min_{\mathcal{S}_1^*}\hat{\mathcal{R}}_H=\min\Big(a,\sqrt[3]{\pi^2a^2b}\Big)=\min\Big(a,\sqrt[3]{\ell_s^2/\ell^2}\Big) \tag{113}$$

so that, regardless of the number and types of disjointed localizations,

$$\min_{\mathcal{S}_1}\mathcal{R}(\tilde{u},\tilde{\alpha})>1$$

since both a and ℓ_s^2/ℓ^2 are greater than one. Hence, localized solutions, when admissible, are always stable in sense of (DS).

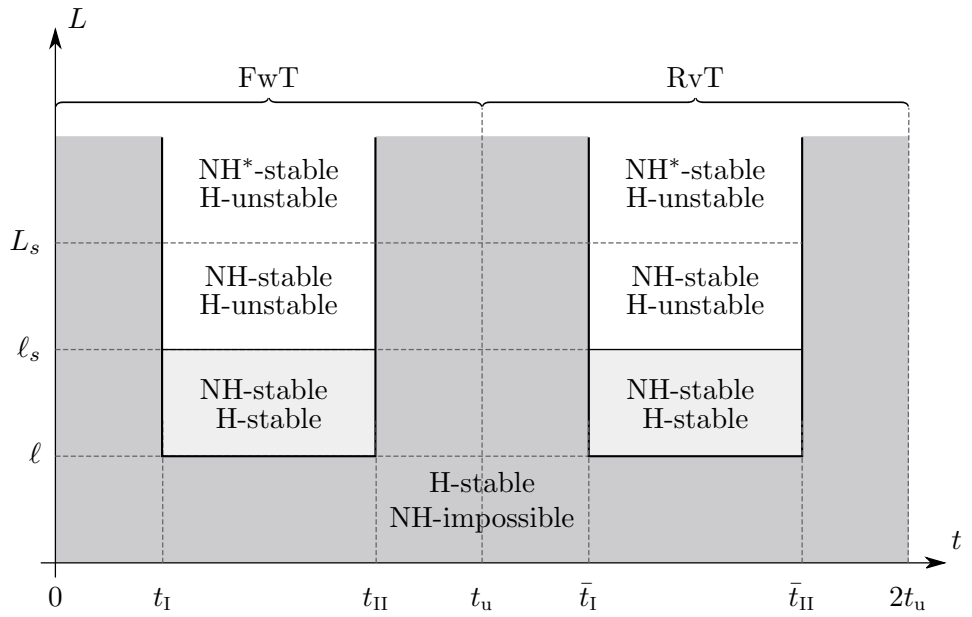

Figure 12: Stability diagram for the homogeneous (H-) and non-homogeneous (NH-) evolutions. The star symbol (*) denotes the occurrence of a snap-back in the response.

Accordingly to this last result and summing up (86), (88) and (107), one can conclude that, depending on the bar length, different types of stable responses may occur, which are likely to be observed, Tab. 1 and Figure 12. In particular, for $\ell \leq L < \ell_s$, the investigation of the transition from a homogeneous solution to a non-homogeneous solution (bifurcation problem) is similar to [38] in the context of damage mechanics but is out of scope in this paper.

$L < \ell$	homogeneous response
$\ell \leq L < \ell_s$	homogeneous or non-homogeneous response without snap-back
$\ell_s \leq L < L_s$	non-homogeneous response without snap-back
$L_s \leq L$	non-homogeneous response with snap-back

Table 1: Stable responses which are likely to be observed depending on the bar length during the phase transformation.

9. Experiments comparison

The model discussed in the previous Sections is now validated against some experimental data, taken from [21] due to the accurate experimental setting which allows one to observe the stress nucleation peaks as well as the evolution of the transformation fronts.

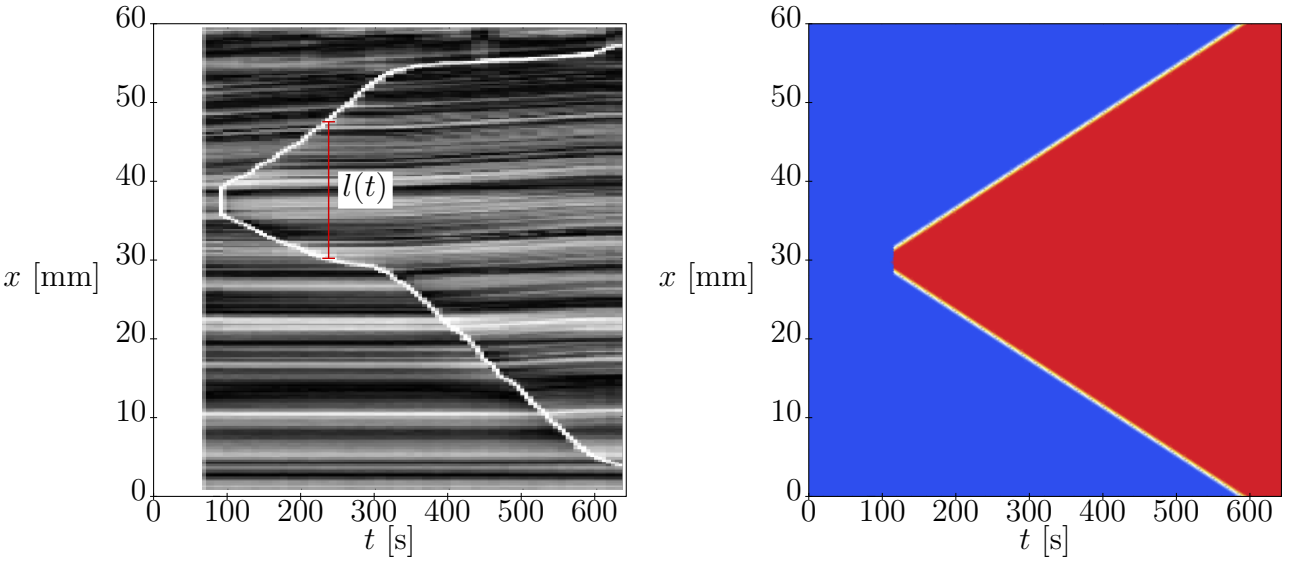

(a) Experimental optical images with front motion highlighted in red for clarity.

(b) Analytical Phase fraction evolution (Blue, $\alpha = 0$; Red, $\alpha = 1$).

Figure 13: FwT Transformation.

The specimen is a 60 mm sample of a 0.76 mm diameter superelastic Nitinol wire. The wire, which is initially unstretched in pure austenite, is monotonically loaded by applied displacements at an average strain rate of $\dot{U}(t)/L = 10^{-4}\mathrm{s}^{-1}$ slow enough to ensure almost isothermal evolution at a temperature of $T = 24.0\,^{\circ}\mathrm{C}$. Before the beginning of the loading, a local heating is artificially imposed at both extremities of the bar, producing local temperature gradients that inhibit nucleations at the grips that would otherwise be triggered by the stress concentrations. This creates the conditions for the nucleation of an inner localization close to the middle of the wire, as shown by optical images reported in Figure 13a.

The two fronts associated with the inner localizations then propagates towards the ends of the bar. The loading is stopped when the two fronts enter the regions where the temperature gradients are applied. The temperature near the grips is then artificially lowered before unloading in order to be able to stop the reverse propagation of the FwT fronts until the creation of the conditions for the nucleation of a RvT inner localization close to the middle of the wire. The RvT then proceeds with four propagating fronts (Figure 14a).

Transformation stresses and the corresponding average strains are identified from the global response curve of the wire (Figure 15) and are reported in Tab. 2. Similarly, the elastic modulus, that has been assumed equal to the value of pure austenite $E = 46.1$ GPa, is obtained again from the global response curve (Figure 15). The parameters B_T, Ω, Λ_{F} and Λ_{R} are identified from transformation stresses and strains, after assuming $\Lambda_{\mathrm{F}} = -\Lambda_{\mathrm{R}}$ as

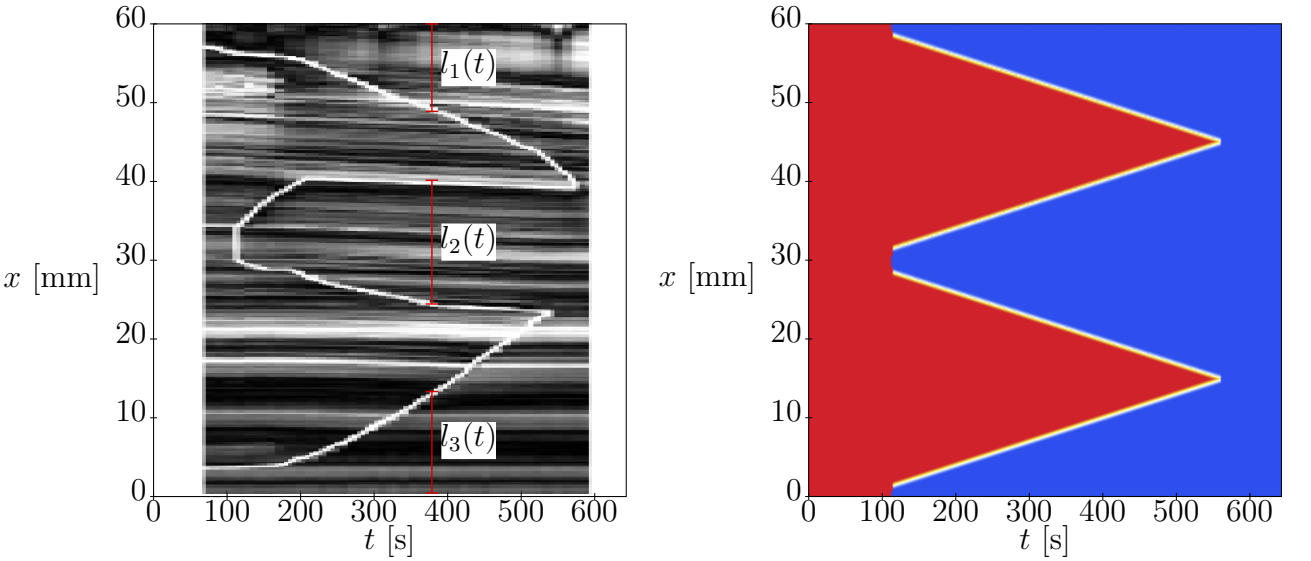

(a) Experimental optical images with fronts motion highlighted in red for clarity.

(b) Analytical Phase fraction evolution (Blue, $\alpha = 0$; Red, $\alpha = 1$).

Figure 14: RvT Transformation.

σ_{M_S}	535 MPa	t_{I}	1.16 %
σ_{M}	441 MPa	t_{II}	5.68 %
σ_{A_S}	138 MPa	$\bar{t}_{\mathrm{I}}$	4.59 %
σ_{A}	225 MPa	$\bar{t}_{\mathrm{II}}$	0.44 %

Table 2: Identified values of the transformation stresses and average strains.

follows

$$\begin{aligned} \sigma_{\mathrm{M}_S} &= (B_T + \Omega + \Lambda)/\mu &&= 535\,\mathrm{MPa} \\ \sigma_{\mathrm{M}} &= (B_T - \Omega + \Lambda)/\mu &&= 441\,\mathrm{MPa} \\ \sigma_{\mathrm{A}_S} &= (B_T - \Omega - \Lambda)/\mu &&= 148\,\mathrm{MPa} \\ t_{\mathrm{IV}} - t_{\mathrm{I}} &= -2\Omega/E\mu + \mu &&= 4.52\,\% \end{aligned}$$

The parameter η has be identified starting from the observation that the nucleation peak in FwT is sharp and then snap-backs occur so that it must be $L > \ell_s$. Moreover, from optical images it is possible to observe a propagation jump of about 2 mm. Using formula (102) it is then possible to compute the value of the snap-back length $L_s = 9.92$ mm, from which, using (106) in the case $n = 1$ and $m = 0$ (that corresponds to the occurrence of a single inner localization) as well together with the definition (84) leads to identify the value for η. The identified constitutive parameters are reported in Tab. 3. The global force-displacement response is shown in Figure 15 where both experimental and analytical curves are compared. The stress drop associated with FwT nucleation is given by $\Omega/\mu = 90.2$ MPa which is in very good agreement with the experimental observation.

B_T	16.5 MPa
Ω	4.42 MPa
Λ	5.32 MPa
μ	0.049
η	0.18 mm

Table 3: Identification of the model constitutive parameters.

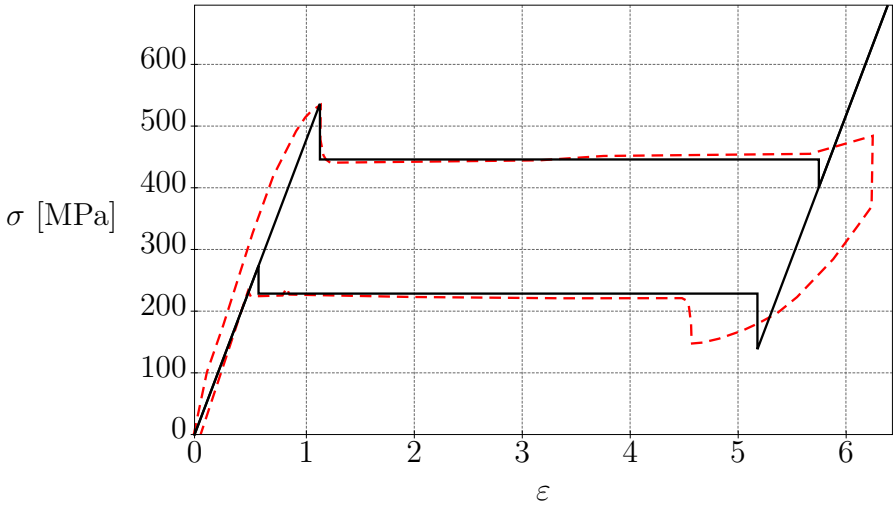

Figure 15: Experimental (dashed-red line) and analytical (solid-black line) global stress-strain response.

The time history of the front propagation predicted by the model in FwT is shown in Figure 13b. The model correctly predicts the extent of the propagation jump and gives a reasonable approximation of the localization nucleation and propagation. The FwT in the modeling reaches its completion just before the end of the loading phase. This is in contrast with the experiments where the loading is stopped when the fronts enter the regions where the thermoelectric wafers used to control the temperature near the ends are located. Therefore FwT comes only close to its completion. This, together the presence of the local temperature gradients, help to explain the less agreement with the observation in this stage of the experiment. The time history of the front propagation predicted by the model in RvT is shown in Figure 14b where an evolution with four fronts is simulated. Again, the model correctly predicts the extent of the propagation jump and gives an approximate symmetrized description of front propagation.

10. Concluding remarks

By the application of a variational formulation based on the three energetic requirements of Irreversibility, Energy Balance and Directional Stability the evolution problem of displacement-controlled tensile tests on SMA wires has been studied.

The analyses show that the occurrence of localized transformations are captured even

by the simplest version of the constitutive model and can be studied in detail, analytically, through a stability analysis. Closed form expressions are obtained for the nucleation and propagation stresses as well as for the localized phase fraction profiles and their spatio-temporal evolution.

A full stability analysis has been carried out for both the homogeneous and non-homogeneous solutions where the role of two internal lengths is highlighted, namely ℓ and ℓ_s which determine respectively the existence of non-homogeneous responses and the stability of the homogeneous response. Moreover the occurrence of snap-back phenomena, which can only occur in non-homogeneous evolutions, is discussed by introducing a third length L_s. It is worth noting that for specific lengths L, such that $\ell \leq L < \ell_s$, both homogeneous and non-homogeneous solutions are allowed.

The analysis of the coalescence explains why the second stress drop associated with the transformation completion is always smaller than the one associated with nucleation and for this reason is more difficult to observe experimentally.

The attention has been restricted to isothermal conditions in order to test the applicability of the approach to model the main phenomena. Forthcoming works will deal with more refined models taking into account the crucial influence of the thermomechanical coupling as well as typical SMA peculiarities like, for example, the heterogeneity of the material properties and variable driving force thresholds.

Acknowledgments

The support provided by the "Istituto Nazionale di Alta Matematica Francesco Severi" (INdAM) through the grant "Progetto Giovani 2014 - GNFM" is gratefully acknowledged.

References

References

[1] Roberto Alessi, Jean-Jacques Marigo, and Stefano Vidoli. Gradient Damage Models Coupled with Plasticity and Nucleation of Cohesive Cracks. *Archive for Rational Mechanics and Analysis*, 214(2):575–615, June 2014.

[2] Roberto Alessi, Jean-Jacques Marigo, and Stefano Vidoli. Gradient damage models coupled with plasticity: Variational formulation and main properties. *Mechanics of Materials*, 80, Part B(0):351–367, 2015.

[3] K M Armattoe, Mohamed Haboussi, and Tarak Ben Zineb. A 2D finite element based on a nonlocal constitutive model describing localization and propagation of phase transformation in shape memory alloy thin structures. *International Journal of Solids and Structures*, 51(6):1208–1220, March 2014.

[4] Nathan J Bechle and Stelios Kyriakides. Localization in NiTi tubes under bending. *International Journal of Solids and Structures*, 51(5):967–980, March 2014.

[5] Davide Bernardini. On the macroscopic free energy functions for shape memory alloys. *Journal of the Mechanics and Physics of Solids*, 49(4):813–837, April 2001.

[6] Davide Bernardini and Renato Masiani. New micromechanical estimates of the interaction energy for shape memory alloys modeled by a two-phases microstructure. *Mathematics and Mechanics of Solids*, pages 1081286514562291–, December 2014.

[7] Davide Bernardini and Thomas J Pence. Models for one-variant shape memory materials based on dissipation functions. *International Journal of Non-Linear Mechanics*, 37(8):1299–1317, December 2002.

[8] Davide Bernardini and Thomas J Pence. ShapeMemory Materials, Modeling. In *Encyclopedia of Smart Materials*. John Wiley & Sons, Inc., July 2002.

[9] Davide Bernardini and Thomas J Pence. Mathematical Models for Shape Memory Materials. In Mel Schwartz, editor, *Smart Materials*. 2009.

[10] B C Chang, J A Shaw, and Mark A Iadicola. Thermodynamics of Shape Memory Alloy Wire: Modeling, Experiments, and Application. *Continuum Mechanics and Thermodynamics*, 18(1-2):83–118, May 2006.

[11] C B Churchill, J A Shaw, and Mark A Iadicola. TIPS AND TRICKS FOR CHARACTERIZING SHAPE MEMORY ALLOY WIRE: PART 3-LOCALIZATION AND PROPAGATION PHENOMENA. *Experimental Techniques*, 33(5):70–78, September 2009.

[12] Hui-Hui Dai and Zongxi Cai. Phase transitions in a slender cylinder composed of an incompressible elastic material. I. Asymptotic model equation. *Proceedings of the Royal Society A: Mathematical, Physical and Engineering Sciences*, 462(2065):75–95, January 2006.

[13] Dorian Depriester, Anne Maynadier, Karine Lavernhe-Taillard, and Olivier Hubert. Thermomechanical modelling of a NiTi SMA sample submitted to displacement-controlled tensile test. *International Journal of Solids and Structures*, 51(10):1901–1922, February 2014.

[14] Arnaud Duval, Mohamed Haboussi, and Tarak Ben Zineb. Modelling of localization and propagation of phase transformation in superelastic SMA by a gradient nonlocal approach. *International Journal of Solids and Structures*, 48(13):1879–1893, June 2011.

[15] B Fedelich and A Ehrlacher. An analysis of stability of equilibrium and of quasi-static transformations on the basis of the dissipation function. *European journal of mechanics. A. Solids*, 16(5):833–855, 1997.

[16] P Feng and Qing-Ping Sun. Experimental investigation on macroscopic domain formation and evolution in polycrystalline NiTi microtubing under mechanical force. *Journal of the Mechanics and Physics of Solids*, 54(8):1568–1603, August 2006.

[17] S Fu, Y Huo, and I Müller. Thermodynamics of pseudoelasticity - an analytical approach. *Acta Mechanica*, 99(1-4):1–19, March 1993.

[18] J F Hallai and Stelios Kyriakides. Underlying material response for Lüders-like instabilities. *International Journal of Plasticity*, 47:1–12, August 2013.

[19] B Halphen and Quoc Son Nguyen. Generlazied Standard Materials. *Journal de Mécanique*, 14(1):39–63, 1975.

[20] Y J He and Qing-Ping Sun. Rate-dependent domain spacing in a stretched NiTi strip. *International Journal of Solids and Structures*, 47(20):2775–2783, October 2010.

[21] Mark A Iadicola and John A Shaw. An Experimental Setup for Measuring Unstable Thermo-mechanical Behavior of Shape Memory Alloy Wire. *Journal of Intelligent Materials Systems and Structures*, 13(2):157–165, February 2002.

[22] Dimitris C Lagoudas, editor. *Shape Memory Alloys: Modeling and Engineering Applications*. Springer, 2008.

[23] Dimitris C Lagoudas, Pavlin B Entchev, Peter Popov, Etienne Patoor, L Catherine Brinson, and Xiujie Gao. Shape memory alloys, Part II: Modeling of polycrystals. *Mechanics of Materials*, 38(5-6):430–462, May 2006.

[24] A A León Baldelli, Corrado Maurini, and Kim Pham. A gradient approach for the macroscopic modeling of superelasticity in softening shape memory alloys. *International Journal of Solids and Structures*, 52:45–55, January 2015.

[25] Valery I Levitas. The postulate of realizability: Formulation and applications to the post-bifurcation behaviour and phase transitions in elastoplastic materials-I. *International Journal of Engineering Science*, 33(7):921–945, 1995.

[26] Christian Lexcellent. *Shape-memory Alloys Handbook*. Wiley-ISTE, 2013.

[27] Jean-Jacques Marigo. Constitutive relations in plasticity, damage and fracture mechanics based on a work property. *Nuclear Engineering and Design*, 114(3):249–272, June 1989.

[28] Alexander Mielke. A Mathematical Framework for Generalized Standard Materials in the Rate-Independent Case. In Rainer Helmig, Alexander Mielke, and Barbara Wohlmuth, editors, *Multifield Problems in Solid and Fluid Mechanics*, volume 28 of *Lecture Notes in Applied and Computational Mechanics*, pages 399–428. Springer Berlin / Heidelberg, 2006.

[29] Alexander Mielke. *Differential, Energetic, and Metric Formulations for Rate-Independent Processes*, pages 87–169. Springer Lecture Notes in Mathematics, 2011.

[30] Alexander Mielke and Florian Theil. On rate-independent hysteresis models. *NoDEA : Nonlinear Differential Equations and Applications*, 11(2):151–189, 2004.

[31] Quoc Son Nguyen. Bifurcation et stabilité des systèmes irréversibles obéissant au principe de dissipation maximale. *Journal de mécanique théorique et appliquée*, 3(1):41–61, 1984.

[32] Quoc Son Nguyen. Stabilité et bifurcation des systèmes dissipatifs standards à comportement indépendant du temps physique. *Comptes rendus de l'Académie des sciences. Série 2, Mécanique, Physique, Chimie, Sciences de l'univers, Sciences de la Terre*, 310(11):1375–1380, 1990.

[33] Etienne Patoor, Dimitris C Lagoudas, Pavlin B Entchev, L Catherine Brinson, and Xiujie Gao. Shape memory alloys, Part I: General properties and modeling of single crystals. *Mechanics of Materials*, 38(5-6):391–429, May 2006.

[34] Henryk Petryk. Incremental energy minimization in dissipative solids. *Comptes Rendus Mécanique*, 331(7):469–474, July 2003.

[35] Henryk Petryk. Thermodynamic conditions for stability in materials with rate-independent dissipation. *Philosophical transactions. Series A, Mathematical, physical, and engineering sciences*, 363(1836):2479–515, November 2005.

[36] Kim Pham. *Construction et analyse de modèles d'endommagement à gradient*. PhD thesis, Université Pierre et Marie Curie, November 2010.

[37] Kim Pham and Jean-Jacques Marigo. Approche variationnelle de l'endommagement : II. Les modèles à gradient. 2010.

[38] Kim Pham, Jean-Jacques Marigo, and Corrado Maurini. The issues of the uniqueness and the stability of the homogeneous response in uniaxial tests with gradient damage models. *Journal of the Mechanics and Physics of Solids*, 59(6):1163–1190, 2011.

[39] K R Rajagopal and A R Srinivasa. On the thermomechanics of shape memory wires. *Zeitschrift für Angewandte Mathematik und Physik (ZAMP)*, 50(3):459–496, May 1999.

[40] Mel Schwartz, editor. *Encyclopedia of Smart Materials vol 1 and 2*. Wiley, 2002.

[41] Mel Schwartz, editor. *Smart Materials*. CRC, 2008.

[42] J A Shaw. Simulations of localized thermo-mechanical behavior in a NiTi shape memory alloy. *International Journal of Plasticity*, 16(5):541–562, April 2000.

[43] J A Shaw and Stelios Kyriakides. Initiation and propagation of localized deformation in elasto-plastic strips under uniaxial tension. *International Journal of Plasticity*, 13(10):837–871, December 1997.

[44] John A Shaw. A thermomechanical model for a 1-D shape memory alloy wire with propagating instabilities. *International Journal of Solids and Structures*, 39(5):1275–1305, March 2002.

[45] John A Shaw and Stelios Kyriakides. Thermomechanical aspects of NiTi. *Journal of Mechanics Physics of Solids*, 43(8):1243–1281, 1995.

[46] John A Shaw and Stelios Kyriakides. On the nucleation and propagation of phase transformation fronts in a NiTi alloy. *Acta Materialia*, 45(2):683–700, 1997.

[47] Zilong Song and Hui-Hui Dai. Closed-form solutions for inhomogeneous states of a slender 3-D SMA cylinder undergoing stress-induced phase transitions. *International Journal of Engineering Science*, 88:40–63, March 2015.

[48] Zilong Song, Hui-Hui Dai, and Qing-Ping Sun. Propagation stresses in phase transitions of an SMA wire: New analytical formulas based on an internal-variable model. *International Journal of Plasticity*, 42:101–119, March 2013.

[49] Qing-Ping Sun and Zhi-Qi Li. Phase transformation in superelastic NiTi polycrystalline micro-tubes under tension and torsionfrom localization to homogeneous deformation. *International Journal of Solids and Structures*, 39(13-14):3797–3809, June 2002.

[50] Qing-Ping Sun, H Zhao, R Zhou, D Saletti, and H Yin. Recent advances in spatiotemporal evolution of thermomechanical fields during the solidsolid phase transition. *Comptes Rendus Mécanique*, 340(4-5):349–358, April 2012.

[51] H Tobushi, K Tanaka, T Hori, T Sawada, and T Hattori. Pseudoelasticity of TiNi Shape Memory Alloy : Dependence on Maximum Strain and Temperature. *JSME international journal. Ser. A, Mechanics and material engineering*, 36(3):314–318, July 1993.

[52] H Ziegler and C Wehrli. The Derivation of Constitutive Relations from the Free Energy and the Dissipation Function. In Theodore Y Wu and John W Hutchinson, editors, *Advances in applied mechanics. Volume 25 (A89-16302 04-39). San Diego, CA, Academic Press, Inc., 1987, p. 183-238.*, volume 25 of *Advances in Applied Mechanics*, pages 183–238. Elsevier, 1987.

Appendix A. Formal integration of the FwT nonlocal criterion

The phase fraction profiles that may occur during FwT can be obtained by evaluating the general integral (87) of the transformation criterion (64) over each interval $\overline{FwT}_i$, together with suitable boundary conditions. The solution (87) has an oscillatory character with extrema taking place at

$$\bar{x} + n\ell \qquad \text{with} \qquad \bar{x} := \frac{\ell}{\pi} \arctan \frac{C_2}{C_1} \tag{A.1}$$

where $\bar{x}$ corresponds to some maximum. Different solutions may arise depending on the geometry of $\overline{FwT}$. In the following the basic situations are illustrated. More general profiles can then be obtained by combining the elementary cases. For illustration see Figure 5 and Figure 6.

A *left boundary localization* arises if $\overline{FwT}$ is of the form $[0, \ell]$. Taking into account (42) it follows that

$$\alpha'_t(0) = 0, \qquad \dot{\alpha}'_t(0) = 0$$

therefore both phase fraction and its rate must take extremum values at the left end of the bar. At the other endpoint it must be

$$\alpha'_t(\ell) = 0, \qquad \dot{\alpha}_t(\ell) = 0$$

due to the spatial continuity of α'_t and the fact that in the adjacent region the phase fraction cannot evolve. It then follows that the region may accommodate one or more spatial oscillations, the minimal case being the one in which an half-oscillation over a length ℓ with a minimum or a maximum the the boundary. Similar considerations hold for a right boundary localization of the form $[L - \ell, L]$ and, overall, there are four basic cases.

- *Left boundary* localization over the interval $[0, \ell]$ matched *with pure austenite* (type a, Figure 5a) characterized by:

  $$\bar{x} = 0, \quad \alpha(\ell) = 0$$

  that gives

  $$C_1 = \frac{\bar{\alpha}_{\mathrm{F}}(\sigma)}{2}, \qquad C_2 = 0$$

  so that

  $$\alpha(x) = \begin{cases} \dfrac{\mu(\sigma_{\mathrm{M}_S} - \sigma)}{\Omega} \cos^2\left(\dfrac{\pi}{2\ell} x\right) & x \in [0, \ell] \\ 0 & x \in [\ell, L] \end{cases} \tag{A.2}$$

  This corresponds to an half-sinusoid with stress-dependent maximum at $x = 0$ and a non-evolving minimum equal to 0 at $x = \ell$. The peak value $\alpha_{max} = \bar{\alpha}_{\mathrm{F}}(\sigma)$ increases with decreasing stress and it is equal to 1 at σ_{M_P} therefore this type of localization may arise for

  $$\sigma_{\mathrm{M}_P} \leq \sigma \leq \sigma_{\mathrm{M}_S}$$

- *Left boundary* localization over the interval $[0, \ell]$ matched *with pure martensite* (type b, Figure 5b) characterized by:

$$\bar{x} - \ell = 0, \quad \alpha(\ell) = 1$$

that gives:

$$C_1 = \frac{\bar{\alpha}_{\mathrm{F}}(\sigma)}{2} - 1, \qquad C_2 = 0$$

so that

$$\alpha(x) = \begin{cases} 1 - \left(2 - \dfrac{\sigma_{\mathrm{M}_S} - \sigma}{\sigma_{\mathrm{M}_S} - \sigma_{\mathrm{M}_P}}\right) \cos^2 \dfrac{\pi x}{2\ell} & x \in [0, \ell] \\ 1 & x \in [\ell, L] \end{cases} \tag{A.3}$$

This corresponds to an half-sinusoid with a non-evolving maximum equal to 1 at $x = \ell$ and a stress-dependent minimum at $x = 0$

$$\alpha_{min} = \frac{\sigma_{\mathrm{M}_P} - \sigma}{\sigma_{\mathrm{M}_S} - \sigma_{\mathrm{M}_P}} \tag{A.4}$$

The minimum increases with decreasing stress and it is equal to 0 at σ_{M_P} while it is equal to 1 at σ_{M_F} therefore this type of localization may arise for

$$\sigma_{\mathrm{M}_F} \leq \sigma \leq \sigma_{\mathrm{M}_P}$$

A *right boundary localization* arises if $\overline{FwT}$ is of the form $[L - \ell, L]$. Similarly to what just discussed, there are two main cases.

- *Right boundary* localization over the interval $[L - \ell, L]$ matched *with pure austenite* (type c, Figure 5c) characterized by:

$$\bar{x} = L, \quad \alpha(L - \ell) = 0$$

that gives

$$C_1 = \frac{\bar{\alpha}_{\mathrm{F}}(\sigma)}{2} \cos\left(\frac{L}{\ell}\pi\right), \qquad C_2 = \frac{\bar{\alpha}_{\mathrm{F}}(\sigma)}{2} \sin\left(\frac{L}{\ell}\pi\right)$$

so that

$$\alpha(x) = \begin{cases} 0 & x \in [0, L - \ell] \\ \dfrac{\mu(\sigma_{\mathrm{M}_S} - \sigma)}{\Omega} \cos^2 \dfrac{\pi(L - x)}{2\ell} & x \in [L - \ell, L] \end{cases} \tag{A.5}$$

This corresponds to an half-sinusoid with stress-dependent maximum at $x = L$ and a non-evolving minimum equal to 0 at $x = L - \ell$. The peak value has the same expression as for type a) hence this localization may arise in the same stress interval;

- *Right boundary* localization over the interval $[L - \ell, L]$ matched *with pure martensite* (type d, Figure 5d) characterized by:

$$\bar{x} + \ell = L, \quad \alpha(L - \ell) = 1$$

that gives

$$\begin{aligned} C_1 &= \left(\frac{\bar{\alpha}_{\mathrm{F}}(\sigma)}{2} - 1\right)\cos\left(\frac{\pi L}{\ell}\right) \\ C_2 &= \left(\frac{\bar{\alpha}_{\mathrm{F}}(\sigma)}{2} - 1\right)\sin\left(\frac{\pi L}{\ell}\right) \end{aligned}$$

so that

$$\alpha(x) = \begin{cases} 1 & x \in [0, L-\ell] \\ 1 - \left(2 - \dfrac{\sigma_{\mathrm{M}_S} - \sigma}{\sigma_{\mathrm{M}_S} - \sigma_{\mathrm{M}_P}}\right)\cos^2\dfrac{\pi(L-x)}{2\ell} & x \in [L-\ell, L] \end{cases} \tag{A.6}$$

This corresponds to an half-sinusoid with stress-dependent minimum at $x = L$ and a non-evolving maximum equal to 1 at $x = L - \ell$. The minimum value has the same expression as for type b) hence the localization may arise in the same stress interval.

An *inner localization* is a connected component of $\overline{FwT}$ of the form $[a, b]$ with a, b points in the interior of the bar. Taking into account boundary conditions, phase fraction must take non-evolving extremum values at the end points of the interval so that $b-a$ must be an even multiple of ℓ, the basic case being a full oscillation over a support of 2ℓ with an evolving maximum or minimum at the midpoint of the interval (the center of the localization). To this end there are two possibilities.

- *Inner localization* from pure austenite (type e, Figure 6a) over an interval $[x_i - \ell, x_i + \ell]$ for some internal point $\ell \leq x = x_i \leq L - \ell$ characterized by:

  $$\bar{x} = x_i, \quad \alpha(x_i - \ell) = 0$$

  that gives

  $$\begin{aligned} C_1 &= \frac{\bar{\alpha}_{\mathrm{F}}(\sigma)}{2}\cos\left(\frac{\pi}{\ell}x_i\right) \\ C_2 &= \frac{\bar{\alpha}_{\mathrm{F}}(\sigma)}{2}\sin\left(\frac{\pi}{\ell}x_i\right) \end{aligned}$$

  so that

  $$\alpha(x) = \begin{cases} 0 & x \in [0, x_i - \ell] \\ \dfrac{\mu(\sigma_{\mathrm{M}_S} - \sigma)}{\Omega}\cos^2\dfrac{\pi(x - x_i)}{2\ell} & x \in [x_i - \ell, x_i + \ell] \\ 0 & x \in [x_i + \ell, L] \end{cases} \tag{A.7}$$

  This corresponds to a sinusoid with two non-evolving minima equal to 0 at $x = x_i - \ell$ and $x = x_i + \ell$ and a stress-dependent maximum at $x = x_i$. The peak value has the same expression as for types a) and c) hence this localization may arise in the same stress interval;

- *Inner localization* from pure martensite (type f, Figure 6b) over an interval $[x_i-\ell, x_i+\ell]$ for some internal point $\ell \leq x = x_i \leq L-\ell$ characterized by:

$$\bar{x} - \ell = x_i, \quad \alpha(\bar{x}) = 1$$

that gives

$$C_1 = \left(\frac{\bar{\alpha}_{\mathrm{F}}(\sigma)}{2} - 1\right) \cos\left(\frac{\pi}{\ell} x_i\right)$$
$$C_2 = \left(\frac{\bar{\alpha}_{\mathrm{F}}(\sigma)}{2} - 1\right) \sin\left(\frac{\pi}{\ell} x_i\right)$$

so that

$$\alpha(x) = \begin{cases} 1 & x \in [0, x_i - \ell] \\ 1 - \left(2 - \dfrac{\sigma_{\mathrm{M}_S} - \sigma}{\sigma_{\mathrm{M}_S} - \sigma_{\mathrm{M}_P}}\right) \cos^2 \dfrac{\pi(x - x_i)}{2\ell} & x \in [x_i - \ell, x_i + \ell] \\ 1 & x \in [x_i + \ell, L] \end{cases} \tag{A.8}$$

This corresponds to a sinusoid with two non-evolving maxima equal to 1 at $x = x_i - \ell$ and $x = x_i + \ell$ and a stress-dependent minimum at $x = x_i$. The minimum value has the same expression as for types b) and d) hence this localization may arise in the same stress interval.